CHALMERS

Cryogenic biogas upgrading using plate heat exchangers

Master's Thesis within the Sustainable Energy Systems Master's programme

SIMON JONSSON

JOHAN WESTMAN

Department of Energy and Environment
Division of Energy Technology
CHALMERS UNIVERSITY OF TECHNOLOGY
Göteborg, Sweden 2011
T2011-350

Cryogenic biogas upgrading using plate heat exchangers

Master's Thesis within the Sustainable Energy Systems Master's programme.

SIMON JONSSON

JOHAN WESTMAN

SUPERVISOR:

Martin Seemann

EXAMINER

Henrik Thunman

Cryogenic biogas upgrading using plate heat exchangers
Master's Thesis within the Sustainable Energy Systems Master's programme
SIMON JONSSON
JOHAN WESTMAN

Cover:
An illustration of a plate heat exchanger from Figure 13. Plate heat exchangers are further described in Chapter 3.4.4.

Cryogenic biogas upgrading using plate heat exchangers

Master's Thesis in the Sustainable Energy Systems Master's programme
SIMON JONSSON
JOHAN WESTMAN
Department of Energy and Environment
Division of Energy Technology
Chalmers University of Technology

ABSTRACT

Cryogenic biogas upgrading has become a fairly discussed concept in the last years. This is mainly due to the possibility to also produce Liquefied Biogas (LBG), which has benefits regarding energy density and transportability. Cryogenic separation processes are generally rather complex and imply relatively large investment costs. This work presents experimental results from a cryogenic biogas upgrading test rig constructed with simple standard components. The aim of the work is to investigate this specific test rig and how the desublimation of CO_2 inside the plate heat exchanger is affected by different operational parameters such as pressure, temperatures and mass flow rates. The goal of biogas upgrading is to produce a gas containing low CO_2 concentration.

Tests showed that it is possible to produce upgraded biogas containing less than 1% CO_2 under continuous operation. The most important factor affecting the heat exchangers ability to desublimate CO_2 is the heat exchanger temperature. Higher biogas flow velocity and shorter residence time results in lower separation efficiency and more evenly distributed CO_2 frost. The biogas pressure and mass flow rate has less impact. With an average heat exchanger temperature of -102 °C the upgraded biogas contained less than 1% CO_2.

A higher biogas pressure results in increased CO_2 desublimation temperature. The outlet CO_2 concentration is lower when running the separation process with higher biogas pressure compared to using a lower pressure. A higher biogas mass flow rate results in slightly higher CO_2 concentration, shorter separation time and with an equal amount of upgraded biogas compared to when using a lower flow rate.

The amount of desublimated CO_2 was between 10.1 and 31.0 grams. The separation proceeded until the heat exchanger either froze up or the CO_2 outlet concentration became too high. The distribution of the desublimated CO_2 was found to be concentrated to the upper parts of the heat exchanger. The regenerative process was shown to take considerably longer time than the separation process itself.

Key words: Biogas upgrading, CO_2 desublimation, Cryogenic separation, Plate heat exchangers

Kryogen uppgradering av biogas med plattvärmeväxlare
Examensarbete inom masterprogrammet Sustainable Energy Systems
SIMON JONSSON
JOHAN WESTMAN
Institutionen för Energi och Miljö
Avdelningen för Energiteknik
Chalmers tekniska högskola

SAMMANFATTNING

Kryogen uppgradering av biogas har under senaste åren diskuterats allt mer. Det är främst möjligheten att framställa flytande biogas som gjort att tekniken hamnat i fokus. Flytande biogas är lättare att transportera och energidensiteten är hög jämfört med komprimerad biogas. Kryogen teknik är relativt tekniskt avancerad och medför normalt stora investeringskostnader. I detta arbete presenteras experimentella resultat från en testrigg byggd av standardkomponenter. Syftet med arbetet är att undersöka hur olika parametrar såsom temperatur, tryck och massflöde påverkar desublimeringen av CO_2 inuti värmeväxlaren. Målet med biogasuppgradering är att producera en gas innehållande låg koncentration av CO_2.

Tester visade att uppgraderad biogas med mindre än 1 % CO_2 kan produceras under ett kontinuerligt förlopp. Den faktor som har störst inverkan på värmeväxlarens förmåga att desublimera CO_2 är dess temperatur. Högre flödeshastighet på biogasen och kortare uppehållstid resulterar i lägre separationseffektivtet och en mer utbredd fördelning av utfrusen koldioxid. Trycknivån och massflödet hos inkommande biogas har mindre påverkan på dessa egenskaper. Då värmeväxlarens medeltemperatur var -102 °C uppmättes CO_2-koncentrationen till mindre än 1 % hos den uppgraderade biogasen.

Ett högre tryck på inkommande biogas resulterar i att koldioxidens desublimerings-tempertatur ökar. Den utgående CO_2-koncentrationen blir lägre då processen körs med högre biogastryck. Ett ökat massflöde av inkommande biogas resulterar i en något högre CO_2-koncentration och kortare avskiljningstid, dock med samma mängd uppgraderad biogas som resultat.

Mängden CO_2 som desublimerades var mellan 10,1 och 31,0 gram. Avskiljningen fortskred i samtliga fall tills dess att värmeväxlaren frös igen eller att CO_2-koncentrationen hos utgående biogas blev för hög. Fördelningen av desublimerad CO_2 visade sig vara koncentrerad till värmeväxlarens övre hälft, och regenereringen av värmeväxlaren tog betydligt längre tid än själva avskiljningen.

Nyckelord: Uppgradering av biogas, Desublimering av CO_2, Kryogen avskiljning, Plattvärmeväxlare

Contents

IV

Preface

In this thesis work, experimental studies have been performed using a custom built demonstrational test rig. The tests have been carried out from January 2011 to May 2011. This work is the mandatory last part for the degree of Master of Science. The project was carried out at the division for Energy Technology at the department of Energy and Environment, Chalmers University of Technology, Sweden. The idea for this thesis originates from Göteborg Energi AB, who also financed the experimental studies. The test rig was designed by TecNet Nordic AB.

The work has been supervised by Martin Seemann and examined by Henrik Thunman. All experimental tests have been performed in the laboratory belonging to the division of Energy Technology at Chalmers University of Technology. We would like to especially thank the Ph. D. students working in the laboratory for their help with setting up the gas analyzers.

Göteborg May 2011

Simon Jonsson

Johan Westman

Notations

Abbreviations

CBG	Compressed Biogas (~200 bar)
CFB	Circulating Fluidized Bed
ESA	Electric Swing Adsorption
HHV	Higher heating value
HX A	Heat exchanger A
HX B	Heat exchanger B
LBG	Liquefied Biogas
LCNG	Liquid to Compressed Natural Gas
LFG	Landfill gas
LNG	Liquefied Natural Gas
LPG	Liquefied Petroleum Gas
MEA	Mono-Ethanol Amine
NDIR	Nondispersive Infrared Sensor
PEG	Poly Ethylene Glycol
PSA	Pressure Swing Adsorption
PVA	Poly Vinyl Alcohol
SNG	Synthetic Natural Gas
TSA	Temperature Swing Adsorption
VOC	Volatile Organic Compound

Chemical abbreviations

CH_4	Methane
CO	Carbon monoxide
CO_2	Carbon dioxide
H_2	Hydrogen
H_2O	Water
H_2S	Hydrogen sulphide
N_2	Nitrogen

Letters

α	Heat transfer coefficient	$[W*m^{-2}K^{-1}]$
β	Inverse mean fluid temperature	$[K^{-1}]$
λ	Heat conductivity	$[W*m^{-1}K^{-1}]$
η_d	Desublimation efficiency	$[-]$
μ	Dynamic viscosity	$[N*s*m^{-2}]$
ρ	Density	$[kg*m^{-3}]$
σ	Thermal diffusivity	$[m^2s^{-1}]$

ν	Kinematic viscosity	$[m^2 s^{-1}]$
A	Cross-sectional area in heat exchanger	$[m^2]$
b	Plate spacing	$[m]$
c	Gas concentration	$[kg*m^{-3}]$
C_p	Specific heat	$[J*kg^{-1} K^{-1}]$
D_{AB}	Mass diffusion coefficient	$[m^2 s^{-1}]$
D_e	Equivalent diameter	$[m]$
f	Friction factor	$[-]$
g	Gaseous phase	
G	Gravitational acceleration	$[m*s^{-2}]$
h	Heat transfer coefficient	$[W*m^{-2} K^{-1}]$
h_D	Mass transfer coefficient	$[m*s^{-1}]$
i	Heat of phase change	$[J*kg^{-1}]$
j_H	Friction factor	$[-]$
l	Liquid phase	
$\dot{m}$	Mass flow rate	$[kg*s^{-1}]$
Nu	Nusselt number	$[-]$
p	Pressure	$[Pa]$
P	Partial pressure	$[Pa]$
P	Perimeter of flow passage in heat exchanger	$[m]$
Pr	Prandtl number	$[-]$
Q	Heat flow	$[W]$
r	Specific gravity	$[-]$
R	Gas constant	$[J*kg^{-1} K^{-1}]$
R_f	Fouling factor	$[m^2 K*W^{-1}]$
Ra	Rayleigh number	$[-]$
Re	Reynolds number	$[-]$
Sc	Schmidt number	$[-]$
Sh	Sherwood number	$[-]$
t	Plate thickness	$[m]$
T	Temperature	$[K]$
$\bar{u}$	Mean flow velocity	$[m*s^{-1}]$
U	Overall heat transfer coefficient	$[W*m^{-2} K^{-1}]$

$\dot{V}$	Volumetric flow rate	$[m^3 s^{-1}]$
x	Distance onto heat exchanger	[m]
x_0	Distance until frost point	[m]
y	Mole fraction of specie in gas mixture	[-]
Y	Mass fraction of specie in gas mixture	[-]
W_m	Wobbe index	$[MJ*m^{-3}]$

1   Introduction

Biogas is produced from food residues, sewage waste, waste wood from forest industry etc. The biogas is produced in digestion chambers under anaerobic conditions. The gasification process is more thoroughly described in Chapter 2. Biogas is mainly a mixture of methane (CH_4) and carbon dioxide (CO_2). In order to use biogas as a fuel for vehicles or large scale power production, by-products and CO_2 have to be removed. This process of CO_2 removal is generally called upgrading. Different upgrading techniques are described in Chapter 2.2. The resulting gas consists mainly of CH_4 and is referred to as *upgraded biogas*. *Natural gas* is similar to upgraded biogas, but it originates from fossil resources. The relatively uncommon upgrading process of cryogenic separation is the main topic of interest in this paper. A substitute to natural gas can also be produced from biomass via a more technically advanced process known as thermal gasification. Thermal gasification is not described in this work, but can be studied in (1).

In order to make production of upgraded biogas economically profitable, optimized methods for both production and transportation must be used. There are several different transportation methods currently used for natural gas and upgraded biogas. When transporting natural gas and upgraded biogas in gaseous phase, pipelines are normally used. New pipelines are expensive and require large biogas and/or natural gas production volumes in order to be profitable. There are however already many existing pipeline grids, where upgraded biogas can be injected and mixed with the natural gas.

Many farms already produce biogas and use it locally without first upgrading it for heat and electricity production. This is primarily done in Germany, and to some extent in Sweden. As the potential biogas volume from farms increase, attention is directed towards small scale production of *upgraded* biogas. Small scale biogas production however requires large investment and transportation costs. It can be advantageous to have both fermentation digesters as well as gas upgrading locally on the farms. This would remove the demand for transportation of residues and low grade gas. There are two main alternatives for storage and transportation of upgraded biogas besides using pipelines; *CBG* and *LBG*. CBG is *compressed upgraded biogas* at a pressure of around 200 bar, still in gaseous phase. LBG is *upgraded biogas* that has been cooled and *liquefied* at temperatures around -161 °C under atmospheric pressure. The main advantage of LBG compared to CBG is that LBG has approximately three times as high density, which has great advantages when it comes to transporting the gas. Another benefit is the reduced need for high pressure storage tanks.

1.1   Purpose

This thesis work was conducted in order to evaluate one specific cryogenic technique as a biogas upgrading alternative. The purpose was to produce results and draw conclusions that could later be used to verify a pre study made regarding one specific cryogenic system, and whether or not to move on to a larger scale production facility.

The thesis work also investigated the difficulties involved with carbon dioxide desublimation in the heat exchanger and the resulting effect on heat transfer properties.

1.2 Method

This thesis work consist of two parts; study of literature and experimental work. Conclusions and discussions based on the experimental results are also presented. The information sources used in this project are all presented in Chapter 0. Literature databases used for literature search were *Science Direct*, *Scopus*, and *Google Scholar*, all three available through Chalmers library.

Experiments were performed using a custom built test rig. It was a small scale model in an early stage of development towards commercial equipment. It was designed to demonstrate and investigate the gas separation function and the effect of different operational parameters such as biogas pressure, biogas mass flow and temperature of the separation heat exchanger. The experiments were conducted in the department laboratory using some existing tools and equipment, such as gas analyzers. A graphical interface used during testing was also developed using National Instruments commercial software LabVIEW®.

1.3 Delimitations

This master thesis did not include the design and construction of a laboratory test rig, solely the testing and evaluation of it. The experimental tests were performed as a parameter study, without the intention of finding an optimal operating point. The experiments concerned the separation of CO_2 from the biogas to produce a clean methane gas stream, and not the production of liquefied methane.

2 Background

Biogas is produced by anaerobic digestion and different gas compositions are received after production. Depending on the purposed usage, the biogas needs to be cleaned and upgraded to a certain purity level. After production, cleaning and upgrading the biogas is stored. This is usually done in the form of compressed biogas and to a smaller extent liquefied biogas.

2.1 Biogas production through anaerobic digestion

Biogas is produced through bacterial degradation of biological material in an oxygen free environment. This process is called anaerobic digestion. The process is controlled by keeping the biological material inside a digestion chamber where temperature and pressure can be adjusted to optimize the proliferation of digestive bacteria. A temperature of 37 °C is normally used for mesophilic digestion, and 55 °C for thermophilic digestion.

The gas leaving the anaerobic digestion chamber consists mainly of methane and carbon dioxide. The composition of the gas depends on the source fermentation material used in the process and how the process is designed. Along with methane and carbon dioxide the gas contains other species, such as water vapor and hydrogen sulphide H_2S. H_2S is very corrosive and the gas therefore needs to be cleaned from this substance (2).

The feedstock for this process is organic materials consisting of fat, proteins and carbon hydrates. This can be sewage waste, manure, rest products from food industry and restaurants etc. Typical values of the gas composition after anaerobic digestion of organic material can be seen in Table 1. In these values, water vapor has already been removed from the gas.

Table 1 Typical gas composition after anaerobic digestion of organic material (2)

Specie	Vol %
Methane	55-80
Carbon dioxide	20-45
Nitrogen	0-1
Oxygen	Traces
Hydrogen	Traces
Sulphide	50-2000 (ppm)

2.2   Biogas upgrading techniques

In order to increase the calorific value of the biogas and to create gas useable as fuel, impurities have to be removed. The goal of the upgrading process is to produce a gas with as high methane concentration as possible. The electrical energy cost for upgrading the gas is typically 3-6% of the calorific value of the upgraded gas, depending on the technique used (3).

There are currently many upgrading techniques commercially available and many are under development. The main different principles of operation are presented in this chapter. Advantages and disadvantages are presented at the end.

2.2.1   Chemical absorption

Carbon dioxide is separated by means of chemical reactions with the addition of absorbents such as MEA. The process is limited in loading and has high energy requirement as well as problems concerning corrosion and degradation. A descriptive process layout of the chemical absorption process can be seen in Figure 1.
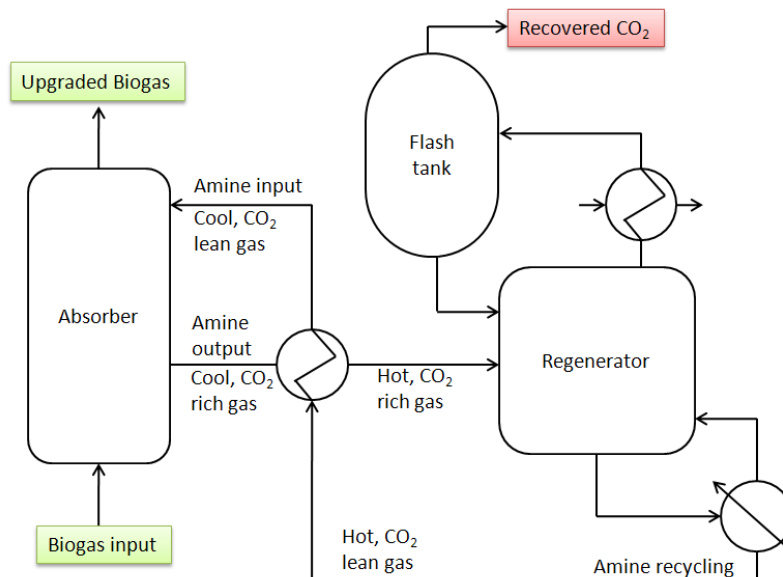
Figure 1 Process schematic of chemical absorption (4)

The biogas flows through the absorber where it is mixed with an absorbent. The CO_2 binds chemically with the absorbent and upgraded biogas consisting of mainly CH_4 leaves the absorber. The upgraded biogas can be purified to CO_2 concentrations below 0.5%. The absorbent is engineered as to only react with carbon dioxide and cannot be used for nitrogen removal e.g. (5). The process is regenerated by submitting the CO_2 rich liquid to a desorber where the temperature is increased. The CO_2 is released from the absorbent which is reused in the absorber. The regeneration requires input of heat, but for cost reasons this is considered preferable compared to replacing the absorbents (4).

The feasibility of small scale chemical absorption of CO_2 was examined in (6). It was concluded that the capacity of the absorbents rapidly decreased and that there were great needs for regeneration. The CO_2 loading for the absorbents ranged from 0.18 to 0.22 kg CO_2 per kg of absorbent. Since the amine solutions showed good regeneration

potential, these were regarded favorable for further studies. The technique of chemical absorption is usually incorporated in larger sized upgrading facilities due to its complexity and cost.

2.2.2 High pressure water scrubbing

High pressure water scrubbing, or wash, is the most common upgrading technique used in Sweden. In high pressure water scrubbing, compressed and cooled biogas enters at the bottom of an absorption column. The gas is then mixed with water which is sprayed from the top of the column. This causes CO_2 and H_2S to solve in the water since their solubility is higher in water than in the biogas. The upgraded biogas then leaves the column. It is then separated from remaining moisture and stored, consisting of up to 98% methane (3).

Two kinds of modifications are normally considered: single-pass scrubbing and regenerative (high pressure) scrubbing. Regenerative scrubbing implies reuse of water, and is often the best option since it results in less water-use. Single-pass scrubbing is normally only feasible if there is an abundance of water available.

As mentioned, the process relies on the solubility of CO_2 and H_2S in water. The reason for compressing the gas before it enters the scrubber is that the dissolubility of the gas increases with increasing pressure. Therefore more CO_2 and H_2S will solve in the water at high pressures, and less water per amount of upgraded gas is needed. An illustration of the water scrubbing process can be seen in Figure 2.
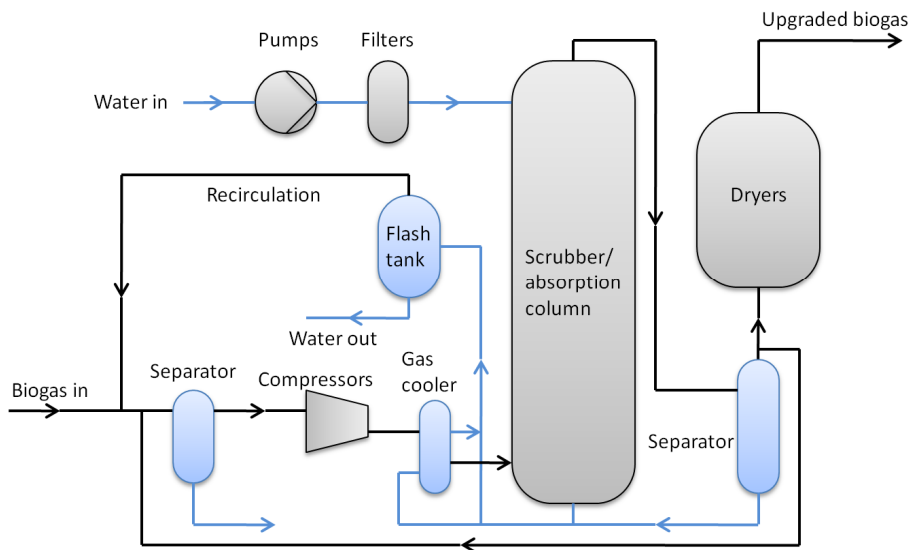
Figure 2 Process schematic of non regenerative water scrubber

High pressure water scrubbing has several features which make it a good option for biogas upgrade:
- It is simple, which means that there are few components needed compared to other upgrade technologies. The equipment also requires little space. Finally, only water is needed as an input
- Wet scrubbers are able to handle high gas temperatures and moist gases
- Wet scrubbers can remove particulate matter and neutralize corrosive gases (7)

2.2.3   Adsorption

Adsorption refers to the process where a specific species is trapped inside a porous material. The porous material, designed with certain porosity, traps molecules of a desired size while letting other molecules pass through unhindered.

There are several different adsorption techniques commercially available for removal of carbon dioxide from biogas. The names of the different techniques indicate the method used to regenerate the adsorption process. Three different methods are described in this section, namely:

- Pressure Swing Adsorption (PSA)
- Temperature Swing Adsorption (TSA)
- Electric Swing Adsorption (ESA)

The currently most used adsorption technique is PSA, where the adsorption takes place at an elevated pressure of about 8 bar. When the species has been adsorbed inside the porous material, the pressure is "swinged" to a lower pressure where the process is regenerated.

The advantages of PSA gas cleaning are that the process does not require any additional chemicals or absorber liquids to operate, and thus has low environmental impact. The power demand for the process is also relatively low, where the energy consumed in the process is used for the compression of the gas before adsorption. The PSA process is illustrated in Figure 3.
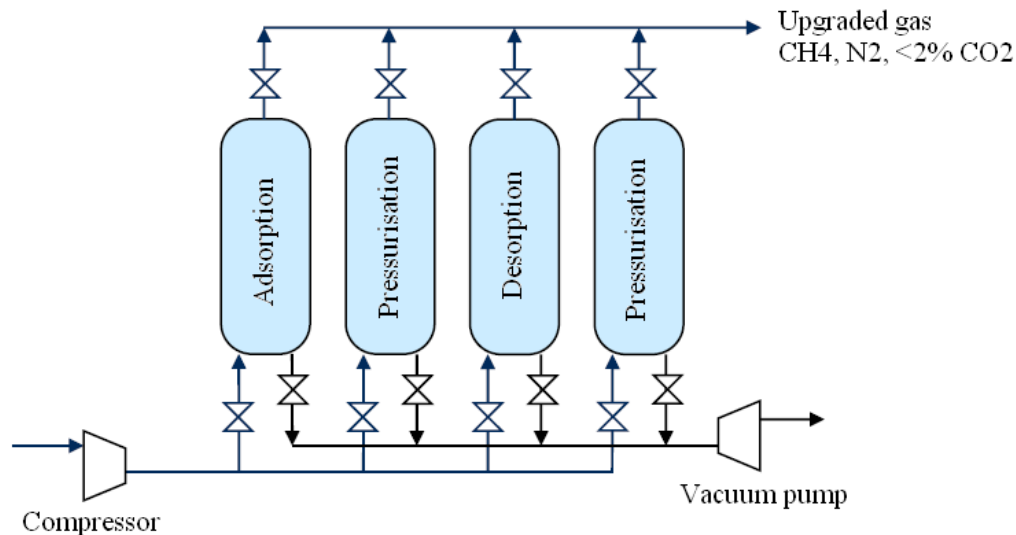
Figure 3 Schematic of a PSA process (5)

TSA works under a different principle. Instead of adjusting the pressure it adjusts the temperature. The technique is usually applied to gas drying, where the moisture is first adsorbed at around 40 °C and the process regenerates at temperatures above 120 °C (5).

Similarly to TSA, Electric Swing Adsorption regenerates by the means of temperature increase. In contrast to TSA, ESA uses a low voltage electric current to heat the adsorbing material by the direct Joule effect. The fact that this process cannot use waste heat for the regeneration, in comparison to TSA, is a disadvantage. To its

advantage can be added that it shows higher potential for VOC (Volatile Organic Compounds) removal than TSA (8).

2.2.4 Membrane separation

Separation of methane and carbon dioxide using membrane technology is a technique widely practiced. Many different materials are used for membranes, but the basic idea is the same. Membranes are either dense and non-porous or made up of hollow fibers. The idea rests on the fact that gases dissolve and diffuse into polymeric materials. The rate of the diffusion is dependent on the size of the molecule (9). The molecules of CO_2 are larger than molecules of CH_4. Polymeric film with pores of certain size will allow the larger CO_2-molecule to pass through the membrane at a much higher rate. The driving force is a pressure gradient applied over the membrane by compression of the incoming gas. The result will be two sets of gases, one rich on CH_4 (levels up to 98%) and one rich on CO_2.
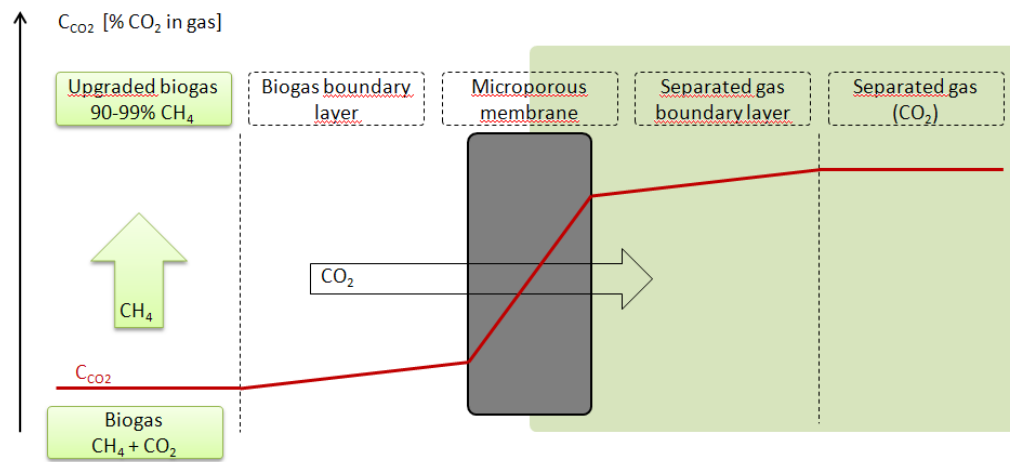
Figure 4 Schematic picture of membrane separation (10)

Primary membrane technology advantages include low energy consumption, absence of moving parts (which implies little risk of fatigue and breakage), low level of mechanical wear and low maintenance level. Also, the set up is light-weight and compact (7).

The membrane's resistance to breaking due to the pressure gradient is one important technical limitation. Exposure to certain solvents and materials causes the membrane to get either damaged or blocked up. These limitations are of great importance since membranes usually are expensive. There are numerous materials investigated for the purpose of membrane production. Some of them are products of Polyimide (9) and PVA/PEG (Poly Vinyl Alcohol/Poly Ethylene Glycol) (11).

2.2.5 Cryogenic separation

The term cryogenic refers to the science of very low temperatures. Cryogenic separation uses the different temperature related properties of the gas species to separate them from each other. In biogas upgrading, the technique is used to create a gas or liquid containing mostly methane and lighter hydrocarbons. An example of a process schematic of a cryogenic upgrading plant is shown in Figure 5. The process starts with the compression of the biogas to approximately 80 bar. Several different heat exchanger steps are used to progressively cool the biogas to a lower temperature,

allowing for the CO_2 to be liquefied and separated. A simpler construction used in this master thesis work can be seen in Figure 15.
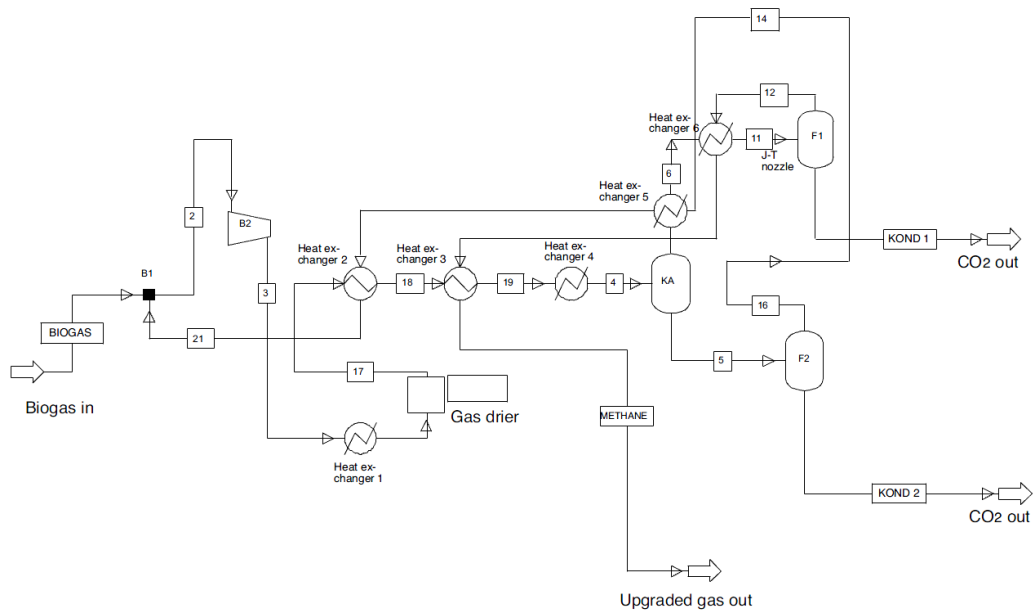
Figure 5 Cryogenic upgrading process schematic (12)

Pure carbon dioxide has a desublimation temperature of -78.5 °C at atmospheric pressure, while methane condenses at -161 °C. CO_2 can be separated by adjusting the temperature of the gas in order to condense or desublimate CO_2. Upgraded biogas without carbon dioxide is then received (13). Depending on the temperature of the process different purity grades can be reached. A lower temperature results in a higher removal efficiency of carbon dioxide.

An advantage of the cryogenic technique is that it does not need any water or absorbent to function, although it requires external cooling equipment such as a refrigeration cycle or the addition of liquid nitrogen.

2.2.6 Comparison of different upgrading techniques

Table 2 provides an overview of the different upgrading techniques. "CH_4 conc." indicates the concentration of methane in the upgraded gas. "CH_4 slip" indicates the amount of methane lost in the process. "H_2S separation" indicates the need of extra process steps to remove H_2S from the biogas. "Process requirements" lists substances consumed during the process, such as water and amines.

8

Table 2 Comparison of different upgrading techniques with respect to CH_4 concentration, CH_4 slip, H_2S separation and requirement of additional fluids (3)

Separation Technique	CH_4 conc.	CH_4 slip	H_2S separation	Process requirements
Chemical Absorption	>99.5% [5], 95-98% [12]	0.1-0.2%. Amines reacts only with CO2	Needed. Done by water scrubbing or additional absorption	Refill of amines
HP Water Scrubbing	96-98% [12], >98% [5]	Re-circulating water: 10-20% (High p → higher solubility of CH_4 in water). Flow through scrubber: 2%	Done in the process. H_2S is later removed in a separate step	Large water requirements, both for single pass and re-circulated water systems. Refill of drying substance for dryers as well as "foam reducing substance"
Adsorption (PSA TSA)	98% [5], 95-98% [12]	PSA: approximately 2%	Done in the process. H_2S is later taken out in a separate step	
Membrane separation	90- 93.5% [9], 98% [14], 76-95% [12]	10-6.5% [9], 2% [14]	H_2S (and water) separated before process due to risk of membrane corrosion	Changing of membranes
Cryogenic separaion	>97% [12]		Required prior to separation process	

Apart from the listed substances, lubricants, glycol, filters and substances for odourization needs to be refilled in all technologies. H_2S separation material such as activated carbon or metal oxides also needs replacement.

Table 3 contains the energy demand for each upgrading technique. The calorific value of upgraded biogas (100% CH_4) is 33.41 MJ/m_n^3, or 9.28 kWh/m_n^3. This is compared to the energy required for upgrading in column 4.

Table 3 Comparison of heat and electricity demand for separation techniques (3)

Separation Technique	Electricity demand [kWh/m_n^3 upgraded biogas]	Heat demand [kWh/m_n^3 upgraded biogas]	Upgrading energy / CH_4 calorific value [%]
Chemical Absorption (with amines)	0.18 [15]	0.20 [15]	2.0
HP Water Scrubbing	Re-circulating: 0.30 Single pass: 0.40-0.50	None	3.2, 4.3-5.4
Adsorption (PSA)	0.50-0.60, 0.29-0.43 [5]	None	5.4-6.5, 3.1-4.6
Membrane separation	0.26 [14]	None	2.8
Cryogenic Separation	0.63, 0.42 [16]	None	6.8, 4.0

The energy required for upgrading is an important parameter in the choice of upgrading technology. HP water scrubbing, adsorption, membrane separation and cryogenic separation are all highly dependent on electricity. Another important parameter is the availability of excess heating and cooling. If there is excess heating available from nearby sources, this heat can with advantage be used for regeneration in e.g. MEA absorption.

Chemical absorption is dependent on the availability of heat. Using MEA as absorbent, the regeneration requires heat at around 120 °C. This makes the technique a good choice when there is excess heat available (15). Another absorbent used is ammonia. Ammonia absorption requires absorber temperatures of 0-10 °C. This implies a need for cooling; both for the absorbing ammonia and the incoming biogas. It is advantageous to integrate ammonia absorption into a process with excess cooling.

The cryogenic separation electricity demand 0.63 kWh/m_n^3 upgraded biogas was calculated using a one stage propane heat pump cycle operating between -100 °C and 40 °C. The process energy demand was 580.9 kJ/m_n^3 upgraded biogas.

Cryogenic separation produces CH_4 at much lower temperatures than other upgrading technologies. The separation can be run at high pressures in order to increase efficiency and to increase the pressure of the output CH_4. Since the CH_4 is cold and at an elevated pressure, the additional energy required for liquefaction is lower than for other technologies. This is the main advantage of cryogenic separation.

2.3 Biogas transport and distribution

Biogas is produced, stored and used in both gaseous and liquid form. CBG can be transported either using available natural gas grids or by trucks. Using the grid is the most favorable option for CBG, but the availability is then limited to locations connected to the grid. Expanding the grid is expensive. In order to facilitate transport and distribution, an alternative is to produce biogas in liquid form, i.e. LBG.

The major advantage of LBG compared to CBG is that LBG takes up considerably less space. Therefore it is more efficient to transport LBG than CBG by trucks. For the same reason, LBG is the better option when shipping biogas overseas. LBG also opens for new biogas applications, for example as a fuel in heavy duty vehicles using Diesel-Methane engines (17). In order for the transport sector to be able to use LBG the fuel needs to be transported over the entire country, primarily using trucks.

Cryogenic upgrading has the possibility to produce LBG directly as a part of the upgrading process. Cryogenic technology is also the only option available for production of LBG from CBG. It is therefore argued that the cryogenic upgrading method has got an advantage compared to the other upgrading technologies (18).

LBG can be produced from CBG at the distribution location. This is done by a so called "MR-station" ("Mät- och reglerstation" in Swedish, which basically translates to "measurement and control facility"). When CBG leaves the grid and enters the distribution station, there is a drop in pressure and temperature. The MR-station utilizes this to produce LBG.

There are also distribution stations that produce CBG from LBG. These stations are called "LCNG stations" (Liquid to Compressed Natural Gas stations) and are commercially available (18).

2.3.1 Pipeline transport

Upgraded biogas can be transported in existing natural gas grids. Grid transport is strictly limited geographically due to the high costs related to natural gas grid expansion. Natural gas grids can be owned either locally by the municipality, nationally by the state or by a commercial actor (19), (12).

Before the upgraded biogas is injected into a natural gas grid it is modified in order to meet the requirements. These include odourization, moisture content, air input mixing, calorific value and *Wobbe index* (12). The Wobbe index is used as a measure of quality, i.e. the energy density of the gas. When switching between different gaseous fuels in burners, the Wobbe index is used to match the combustion properties of the different gases. The Wobbe index W_m is defined as

$$W_m = \frac{HHV_m}{\sqrt{r_m}} \qquad \text{\{Eq. 1\}}$$

where HHV_m is the higher heating value of the gas, and r_m is the specific gravity (or specific density). The higher heating value is defined as

$$HHV_m = \sum_i x_i HHV_i \qquad \text{\{Eq. 2\}}$$

where x_i is the mass fraction of component i and HHV_i is the higher heating value of component i (20). According to (21), the higher heating value HHV_i for a substance is defined as "… the heat release per unit mass when the fuel, initially at 25°C, reacts completely with oxygen and the products are returned to 25°C. The heating value is reported as *higher heating value* (HHV) when the water is condensed …".

The specific gravity r_m is the ratio of gas density to the density of a reference substance. Water is usually used as a reference, and the same surrounding conditions (pressure and temperature) are used for both the liquid and the gas (20).

2.3.2 Trailers and overseas transport

The most common way of transporting LBG is by truck, which has been shown to be an economically efficient way of transportation (18). Some special arrangements are required for the transportation of LNG, namely:

1. Transportation in double-wall insulated tanks
2. Presence of two independent pressure relief systems
3. Appropriate hazardous materials markings (19)

Some of the LBG will vaporize due to heat leakage during the transportation. Eventually, the pressure builds up enough to release the safety valve which ventilates the gas out into the surrounding air. This is a problem for three reasons. Firstly, methane has large greenhouse gas potential. Secondly, methane is flammable and a release poses a safety threat if there is risk for ignition. Thirdly, the vaporization of LBG will decrease the level of fluid in the cans, and partially filled cans experience sloshing due to the moving of the transport. Sloshing in partially filled cans can cause breakage due to fatigue. This is a problem to which solutions currently are being developed (22).

3   Cryogenic separation

Cryogenic separation deals with some special properties regarding the thermodynamics of CO_2, i.e. sublimation and desublimation. The concept of cryogenic separation and the phenomenon related to this technique are further explained in this chapter. There are two main working principles for small scale cryogenic biogas upgrading, namely "closed-loop" and "open-loop" cycles.

3.1   Open-loop process

In the open-loop process the biogas is first compressed to a higher pressure. The temperature increases due to the compression. This allows for the gas to be heat exchanged with lower temperature heat sinks such like outdoor air or an external refrigeration cycle. This can be done in several steps at different temperature levels. After the biogas has been cooled it is expanded through a turbine where the pressure and the temperature are decreased. The shaft work produced by the turbine can be used to supply the compressor with a part of its work input. The biogas can this way reach low enough temperatures to begin the condensation or desublimation of CO_2. If the temperature is lowered further to the condensation temperature of methane, LBG can be produced. The process is designed differently depending on whether the goal is to produce LBG or upgraded biogas. One open-loop process is illustrated in Figure 6.
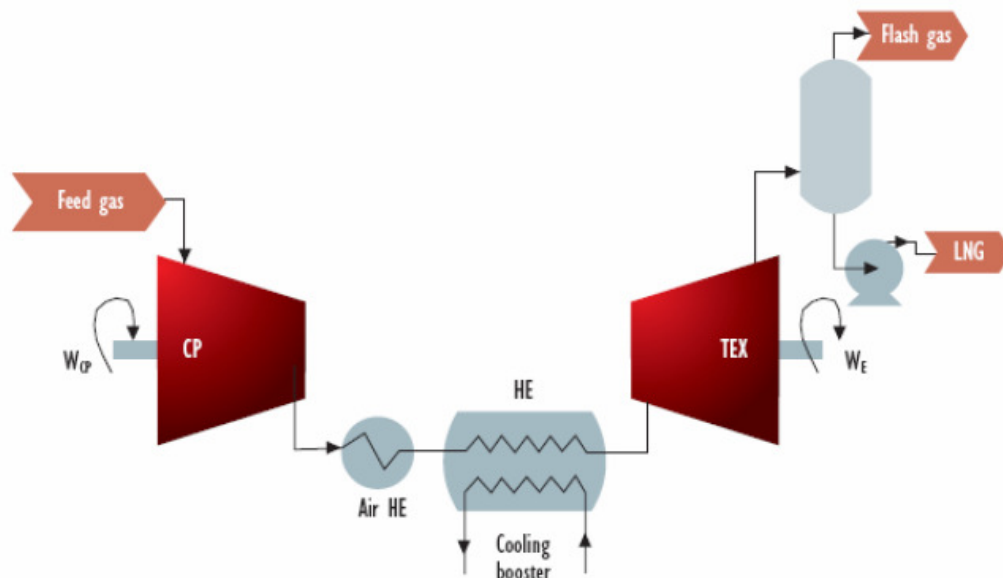
Figure 6 Schematic of open-loop cryogenic process (23)

3.2   Closed-loop process

In this process the biogas is not compressed before being heat exchanged. This results in a lower temperature difference between the two streams. If the temperature of the biogas is not increased via compression, it is not possible to use the air as a heat sink. The cooling process can be driven by different refrigeration cycles using cooling agents e.g. nitrogen and methane, or a mixture of both. The biogas enters the process

and is first cooled by the separate refrigeration process to a low temperature and thereafter expanded through either a valve or a turbine. This decreases both the pressure and the temperature which results in condensation of the methane (23). A scheme of a closed-loop process is illustrated in Figure 7.
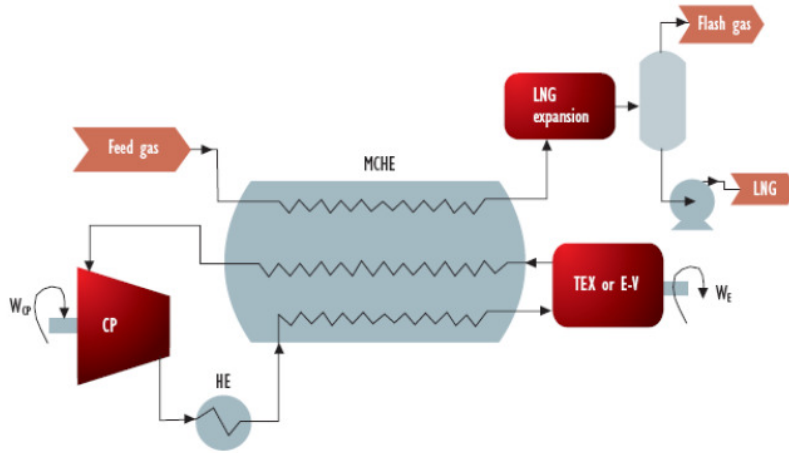
Figure 7 Schematic of closed-loop cryogenic process (23)

3.3 CO$_2$ desublimation

CO$_2$ both desublimate and sublimate under atmospheric pressure, i.e. the CO$_2$ goes straight from gas phase to solid phase and the opposite without first liquefying. The phase diagram for CO$_2$ is shown in Figure 8.
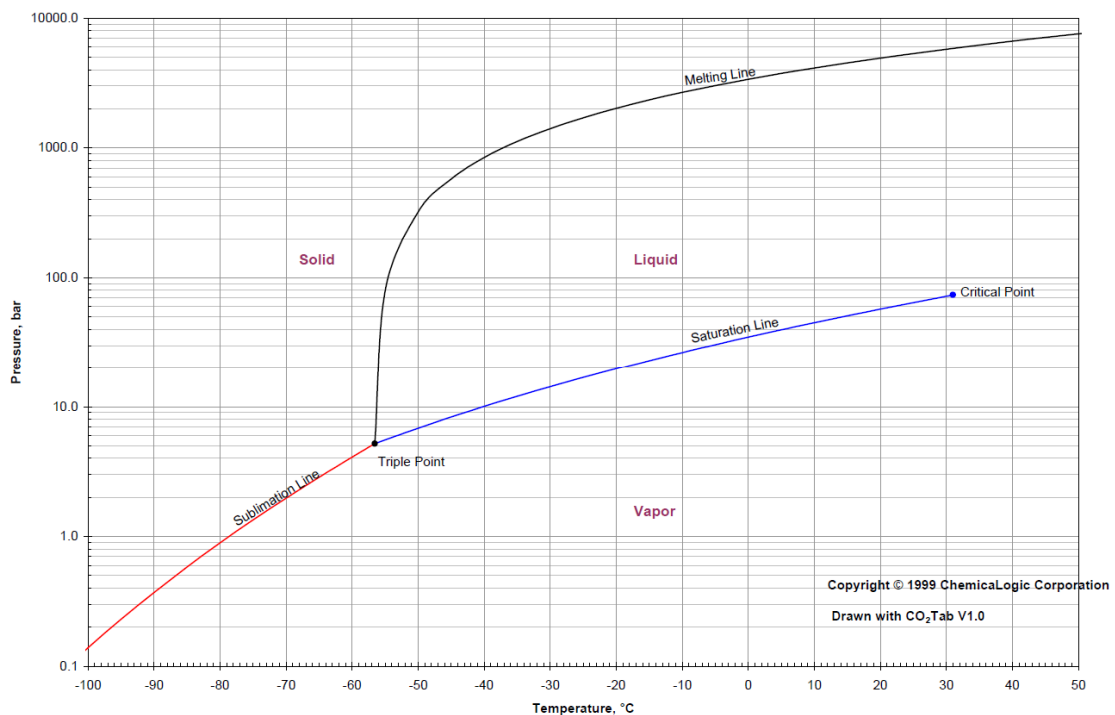
Figure 8 Carbon dioxide phase diagram (24)

Figure 9 shows the saturation pressure of CO_2 at lower pressures. When the CO_2 in the biogas is desublimated it follows that the partial pressure of CO_2 is reduced. This means that as the concentration of CO_2 is lowered, a lower temperature is required in order to further desublimate the CO_2.
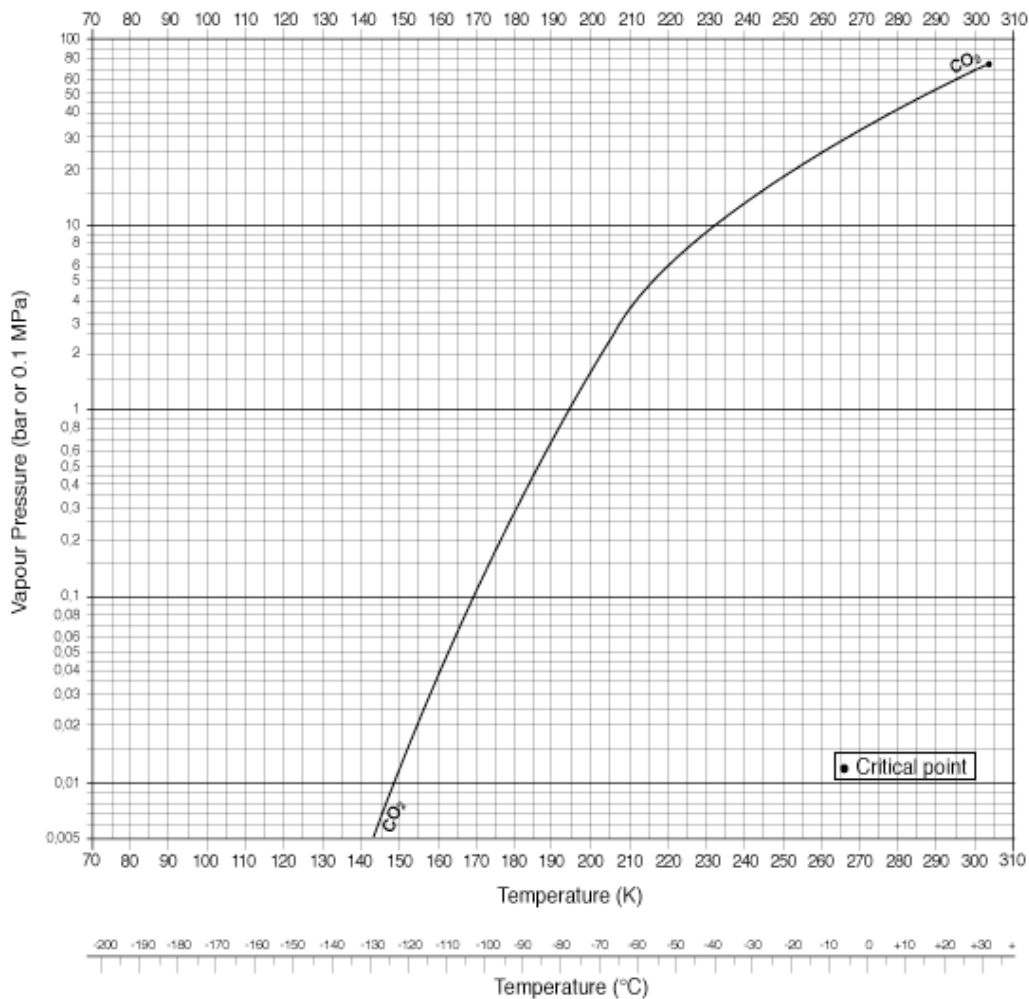
Figure 9 Carbon dioxide vapor pressure (25)

If the biogas is subdued to temperatures to the left of the sublimation line marked in Figure 8 the CO_2 will form frost crystals on the heat exchanger surface. Research regarding the formation of crystallized CO_2 from gas mixtures of CO_2 and N_2 on a longitudinal plate showed that crystals with the size of 0.1-0.5 mm in size formed during the first two minutes of exposure. When increasing the velocity of the biogas, increasing the CO_2 concentration or reducing the plate temperature, larger crystals were formed (26).

When desublimation of CO_2 occurred across the plate there were shown to be differences in the layer thickness across the plate, even though the entire surface of the plate was isothermal. It was shown that the frost layer grew at a greater rate at the leading edge of the plate. This was said to follow from the depletion of CO_2 in the boundary layer further along the plate. This means that the mass transport of CO_2 from the bulk flow to the surface should be considered. The molecular diffusivity of the carbon dioxide in the gas mixture is thus of interest for the desublimation process.

Increasing the velocity of the biogas flow increases the turbulence and thereby also increases the heat and mass transfer.

Schelkunov, Rudenko, Shostak and Dolganin (26) divided the process of CO_2 desublimation into two different periods. Initially there was a rapid frost layer growth with great variations in properties such as density and heat transfer coefficient. During this period the thickness and density of the frost increased rapidly. At the same time the heat and mass transfer coefficients decreased. During the second growth period the properties of the frost layer became more uniform. The thickness, density and thermal conductivity increased at a steady pace. The coefficient of effective thermal conductivity λ was shown to lie between $0.04 - 0.55$ $W*m^{-1}K^{-1}$ (26).

The density of the CO_2 frost layer was investigated under different test conditions in (26). It was shown that the density was somewhere between 500 and 1600 $kg*m^{-3}$ during the first 6 minutes of operation, where the density increased with time. These results were obtained when conducting the tests at 1 to 5 bar pressure, where a higher pressure resulted in a higher frost layer density. A plate temperature of 145 K was used for most of the tests.

Important conclusions regarding the density of the frost layer can be drawn from the results presented in (26).

- A **lower plate temperature** resulted in **higher** frost layer density
- A **lower flow velocity** resulted in **lower** frost layer density
- A **lower pressure** resulted in **lower** frost layer density

Chang, Chung and Park (27) have developed a technique for the upgrading of LFG (Landfill Gas) and the freeze-out of CO_2. A theoretical model for the freeze-out process of CO_2 was presented. Experimental tests to confirm the model were also conducted. The temperature distribution of the incoming gas mixture and the nitrogen can be seen in Figure 10.

The frost layers impact on the heat and mass transfer properties was ignored, under the assumption that the frost layer was never allowed to grow to a significant thickness before the heat exchanger was regenerated.
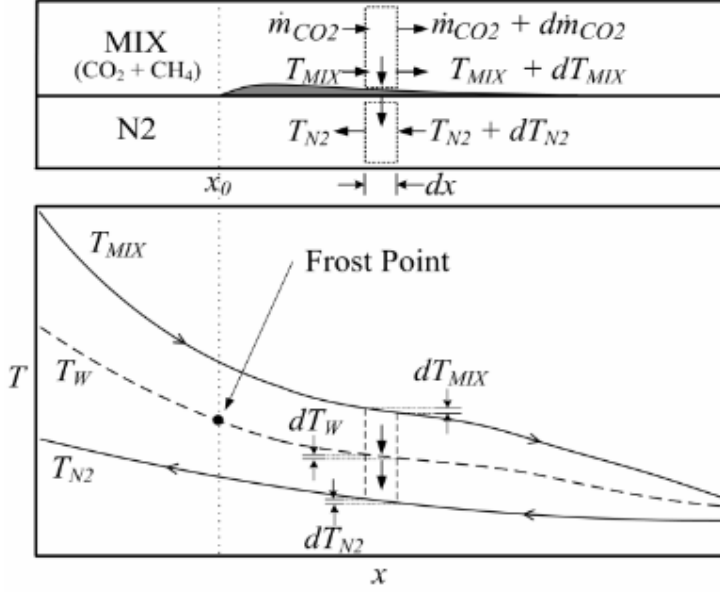
Figure 10 Principle gas mixture temperature distribution (27)

The "Frost Point" refers to the point where the carbon dioxide in the biogas first starts to form a solid layer of frozen CO_2 on the heat exchanger surface. Assuming that the incoming biogas has a composition of only CH_4 and CO_2 and that the cooling media used for the cryogenic separation is liquid N_2, the governing energy balance equations can be written as

$$\left(\dot{m}_{CH4}C_{pCH4} + \dot{m}_{CO2}C_{pCO2}\right)\frac{dT_{MIX}}{dx} = -h_{MIX}P(T_{MIX} - T_W) \qquad \text{\{Eq. 3\}}$$

$$\dot{m}_{N2}C_{pN2}\frac{dT_{N2}}{dx} = -h_{N2}P(T_W - T_{N2}) \qquad \text{\{Eq. 4\}}$$

Where $\dot{m}, C_p$ and h represents the mass flow, the specific heat and the enthalpy. The denomination "mix" refers to the gas mixture of both CH_4 and CO_2. The subscript W refers to the heat exchanger wall between the two media. Two concentrically placed tubes were used as a heat exchanger, where P denotes the perimeter of these. Since the methane in this process is unaffected, the mass balance of methane is given as

$$\frac{d\dot{m}_{CH4}}{dx} = 0 \qquad \text{\{Eq. 5\}}$$

Since the mass flow of carbon dioxide decreases along the heat exchanger length the authors of (27) model the decrease in CO_2 mass flux as

$$-\frac{d\dot{m}_{CO2}}{dx} = \begin{cases} 0 & for\ x<x_0 \\ h_D[c_{CO2} - c_{SAT}(T_W)] & for\ x \geq x_0 \end{cases} \qquad \text{\{Eq. 6\}}$$

Here, h_D refers to the mass transfer coefficient of carbon dioxide in methane. The gas mass concentration is denoted c and x_0 is the frost point location. If the accumulated amount of CO_2 can be considered small, the thermal resistance of the layer can be neglected. This can be the case if the interval between regeneration of the process is short. The main part of the heat transfer between the biogas and the cooling media will be through convection. By also taking into account the phase change energy of the CO_2, the energy balance of the heat exchanger can be described as

$$h_{MIX}P(T_{MIX} - T_W) + i_{ig}\left(-\frac{d\dot{m}_{CO2}}{dx}\right) = h_{N2}P(T_W - T_{N2}) \qquad \text{\{Eq. 7\}}$$

17

Here i_{ig} is the sublimation phase change energy of carbon dioxide. The mass transfer rates can also be described as

$$\dot{m}_{CH4} = c_{CH4}\bar{u}_{MIX}A_{MIX} \tag{Eq. 8}$$

$$c_{CH4} = \frac{P_{MIX}-P_{CO2}}{R_{CH4}T_{MIX}} \tag{Eq. 9}$$

$$\dot{m}_{CO2} = c_{CO2}\bar{u}_{MIX}A_{MIX} \tag{Eq. 10}$$

$$c_{CO2} = \frac{P_{CO2}}{R_{CO2}T_{MIX}} \tag{Eq. 11}$$

where $\bar{u}$ is the mean flow velocity. Here, P denotes the partial pressure of the substances. The heat and mass transfer coefficients can be substituted using empirical correlations by Rhosenow and Choi, giving the following expression

$$\frac{h_{MIX}}{(c_{CO2}+c_{CH4})C_{pMIX}\bar{u}_{MIX}}Pr^{2/3} = \frac{h_D}{\bar{u}_{MIX}}Sc^{2/3} = \frac{f}{2} \tag{Eq. 12}$$

The Prandtl and Schmidt numbers are calculated for the biogas mixture, and the friction factor f depends on the specific geometry of the heat exchanger.

Experiments using biogas with molar fractions of carbon dioxide ranging from 0.1 to 0.3 were performed. It was found that given a higher molar fraction of CO_2 the distance to the first frost formation became longer than when using a lower molar fraction. By adjusting the flow of cooling media the distance to frost formation could also be altered. When using a high cooling media flow the gas mixture was rapidly cooled to sublimation point. Rapid CO_2 accumulation on the heat exchanger was observed. Depending on whether a compact heat exchanger design or a more uniform CO_2 frost layer is desired, the properties can be altered. If a lower cooling media flow is used the accumulation speed will not be as rapid and the layer will become somewhat more evenly distributed. The influence of increasing molar fraction CO_2 in the gas mixture can be seen in Figure 11.
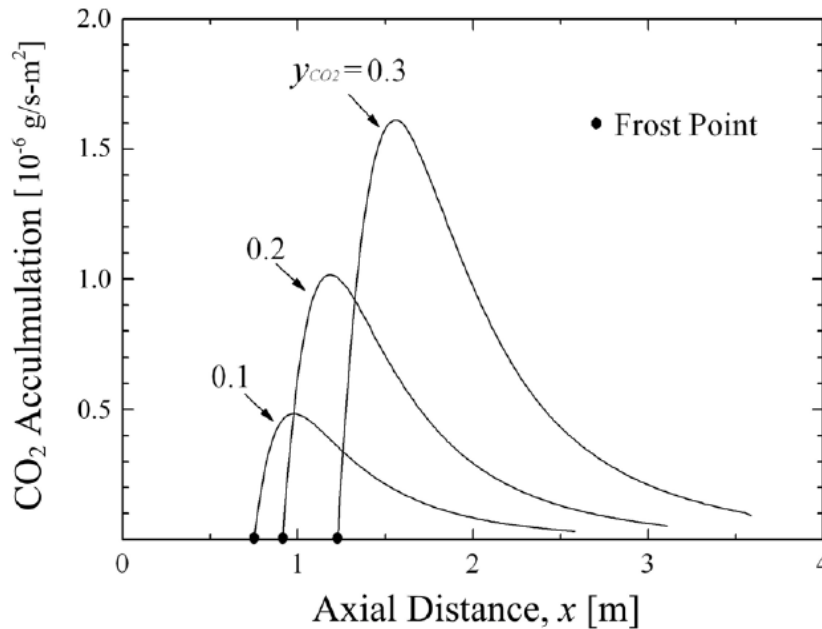
Figure 11 CO$_2$ accumulation rate with different molar fractions of CO$_2$ in gas (27)

The frost point is postponed somewhat due to higher CO_2 concentration in the incoming biogas. This is due to the larger heat capacity C_p per mole CO_2 than mole CH_4.

3.4 Parameters affecting the heat exchanger functionality

Certain parameters have been concluded as influential on the functionality of the heat exchanger. Here, functionality means the heat exchangers ability to separate CO_2 from the biogas. As discussed in Chapter 3.3 the main factors shown to have a large impact on the frost formation are

- Concentration of CO_2 in the incoming biogas
- Temperature of incoming cooling media
- Mass flow of incoming cooling media
- Existing layer of CO_2 already accumulated on surface

Apart from these parameters, an interesting factor to examine is the mass flow of incoming biogas. Additional parameters connected to the heat exchanger size which affect the separation process are

- Total heat exchanger area (which correlates to the size of the heat exchanger)
- Size of heat exchanger plates
- Number of plates in heat exchanger
- Other heat exchanger geometry, such as plate spacing and chevron angles

3.4.1 Concentration of CO_2 in the incoming biogas

An increased CO_2 concentration has in Chapter 3.3 been shown to increase the frost formation closer to the inlet of the biogas. The concentration of CO_2 is higher in the gas stream inlet and so is the amount of CO_2 that comes into contact with the heat exchanger. This results in a higher accumulation rate of CO_2 closer to the inlet. As can be seen from Eq. 6 the mass transfer rate of CO_2 is dependent on the mass transfer coefficient. It can be rewritten as

$$\frac{d\dot{m}_{CO2}}{dx} = -\frac{f * \bar{u}_{MIX}}{2 * Sc^{2/3}} * P * [c_{CO2} - c_{SAT}(T_W)] \qquad \{\text{Eq. 13}\}$$

The Schmidt number is defined as

$$Sc = \frac{\mu}{\rho D_{AB}} = \frac{\nu}{D_{AB}} \qquad \{\text{Eq. 14}\}$$

where D_{AB} is the mass diffusivity of CO_2 in CH_4, μ is the dynamic viscosity and ρ density of the gas. As have been shown in (27) the mass transfer rate of CO_2 is increased with higher concentrations of CO_2 (c_{CO2}) in the gas stream. This can also be seen in Eq. 13.

3.4.2 Temperature and flow rate of incoming cooling media

Decreased temperature of the refrigerant media leads to decreased temperature of the biogas. This results in increased viscosity, increased density and decreased diffusivity within the biogas. The mean flow velocity decreases somewhat due to increased density. As can be seen from Eq. 13 the mass transfer rate of CO_2 is also dependent on the saturation concentration near the wall at temperature T_w. The saturation concentration decreases as the temperature is lowered, resulting in an increased mass transfer rate of CO_2. Thus, a lowered temperature of the cooling media results in a

lower saturation concentration and increased mass transfer. The initial phase of CO_2 accumulation is in some cases influenced by super-cooling, where the temperature of the gas is below the saturation temperature for the gas phase (26). This temperature eventually rises with increasing frost layer thickness to the equilibrium temperature for the phase change. After this the mass accumulation rate is slowed.

The diffusion of CO_2 in CH_4 should be taken into consideration when evaluating the performance of the cryogenic separation. Mass diffusion is according to (28) related to pressure and temperature as:

$$D_{AB} \sim p^{-1}T^{\frac{3}{2}} \qquad \{\text{Eq. 15}\}$$

Using (21) the diffusivity of CO_2 in CH_4 can be approximated for different pressures and temperatures. The binary diffusion coefficient D_0 for CO_2 in CH_4 at $T_0=298K$ and $p_0=100$ kPa pressure is approximately $15*10^{-6}$ m^2s^{-1}. This can be corrected using Eq. 16:

$$D_{AB} = D_0 \left(\frac{T}{T_0}\right)^m \frac{p_0}{p} \qquad \{\text{Eq. 16}\}$$

Where m=1.75 for permanent gases and m=2 for condensable gases, where the latter is closest to the case of desublimation. The process can be designed to run at different pressures. In Table 4 the diffusion coefficients for different biogas temperatures are evaluated using Eq. 16. Values of $T_0=298K$, $p_0=100$ kPa and p=300 kPa are used to illustrate a pressurized process.

Table 4 Coefficients for diffusion of CO2 in CH4 for different mixture temperatures

Biogas temperature [K]	Diffusion Coefficient $D_{AB}*10^6$ $[m^2s^{-1}]$
298	15
280	4.4
260	3.8
240	3.2
220	2.7
200	2.3
180	1.8

The approximated value of the coefficient of diffusion decreases by 88% when the temperature of the gas is lowered from room temperature to 180 K.

In Figure 12 the impact of different cooling media mass flows are displayed. When the mass flow is increased, the frost point and the accumulation peak are pushed towards the biogas inlet. This is due to that the inlet temperature of the cooling media is still constant, thus increasing the heat transfer potential of the cooling stream. This results in a larger temperature difference between the biogas and the refrigerant stream further up the heat exchanger surface.
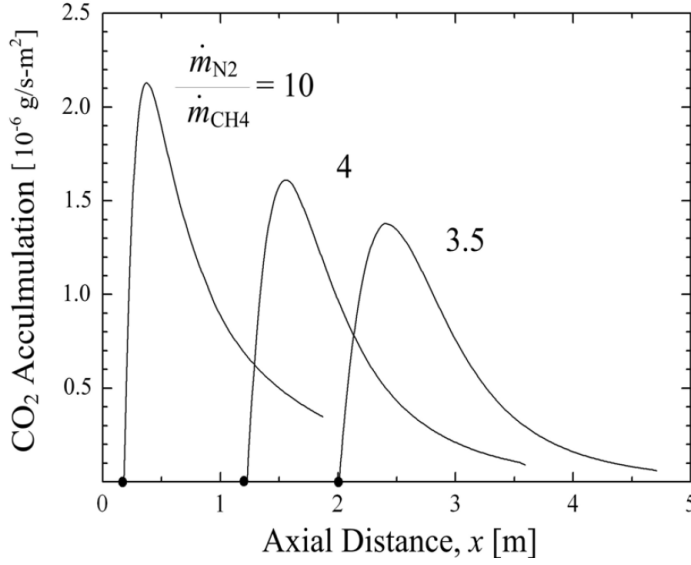
Figure 12 Refrigerant mass flow to biogas mass flow ratio (27)

3.4.3 Mass flow of incoming biogas

When increasing the mass flow of biogas the average flow velocity increases. In turn, an increased flow velocity leads to higher Reynolds numbers. The flow velocity is not determinable in every point, but general expressions can provide an understanding for what happens if it increases. For example, it is suggested by (29) that the Reynolds number for a plate heat exchanger with chevron angle configurations can be approximated as

$$Re = \frac{\rho \bar{u} D_e}{\mu} = \frac{\bar{u} D_e}{\nu} \qquad \text{\{Eq. 17\}}$$

where the equivalent diameter D_e is 2 times the axial spacing of the plates b. As can be seen, an increased flow velocity $\bar{u}$ will increase the Reynolds number. Using convective heat transfer correlations

$$Nu = 0.4 Pr^{0.4} Re^{0.64} \qquad \text{\{Eq. 18\}}$$

or Figure 14 to determine Nu as a function of Re, and

$$Nu = \frac{h D_e}{\lambda} \qquad \text{\{Eq. 19\}}$$

It can be seen that the heat transfer coefficient h is related to Re as

$$h = \frac{\lambda}{D_e} 0.4 Pr^{0.4} Re^{0.64} \qquad \text{\{Eq. 20\}}$$

Hence, an increased flow speed will increase the convective heat transfer. An increased flow velocity will also affect the mass transfer of CO_2 through the biogas towards the heat exchanger wall. Using mass transfer correlations for a flat plate in parallel flow (28) to illustrate the flow across a heat exchanger plate, the correlation between velocity and mass transfer can be approximated. The Sherwood number is defined as

$$Sh = \frac{h_D x}{D_{AB}} = 0.332 Re^{1/2} Sc^{1/3} \qquad \text{\{Eq. 21\}}$$

where x is the distance from the leading edge of the plate. By combining Eq. 14 & 21 and rearranging, the mass transfer coefficient can be expressed as

$$h_D = \frac{0.332}{x} Re^{1/2} v^{1/3} D_{AB}{}^{2/3} \qquad \{Eq.\ 22\}$$

Hence, increased velocity $\bar{u}$ results in an increased mass transfer coefficient h_D, since $Re \sim \bar{u}$ according to Eq. 17 above. Bulk motion and turbulence causes both the heat and mass transfer to increase additionally. An increased flow velocity though results in a shorter residence time, which has negative impact on the total separation efficiency.

3.4.4 Plate heat exchangers

The purpose of heat exchangers is to transfer heat from one fluid to another through a heat exchanger wall. Dealing with temperatures around and below 300K, convective heat transfer is of greater importance than radiative heat transfer. Simulating the heat and mass transfer using only convective heat transfer has proven to produce useful results (27).

The heat transfer properties change as the CO_2 forms a layer of frost on the heat exchanger surface. The "CO_2 frost" builds up gradually. In a first step, sparse crystals form on the surface. As CO_2 continues to accumulate on the surface the frost layer becomes increasingly dense and the thickness increases. At some point, the frost accumulation will prevent the process from proceeding due to lowered heat transfer, "freeze-up" or both (26).

Plate heat exchangers consist of numerous corrugated thin plates stacked on each other. In the experimental rig in this thesis work, liquid nitrogen was heat exchanged with a refrigerant which in turn was heat exchanged with biogas. An illustration of the flow paths within a "one pass/one pass" plate heat exchanger can be seen in Figure 13.
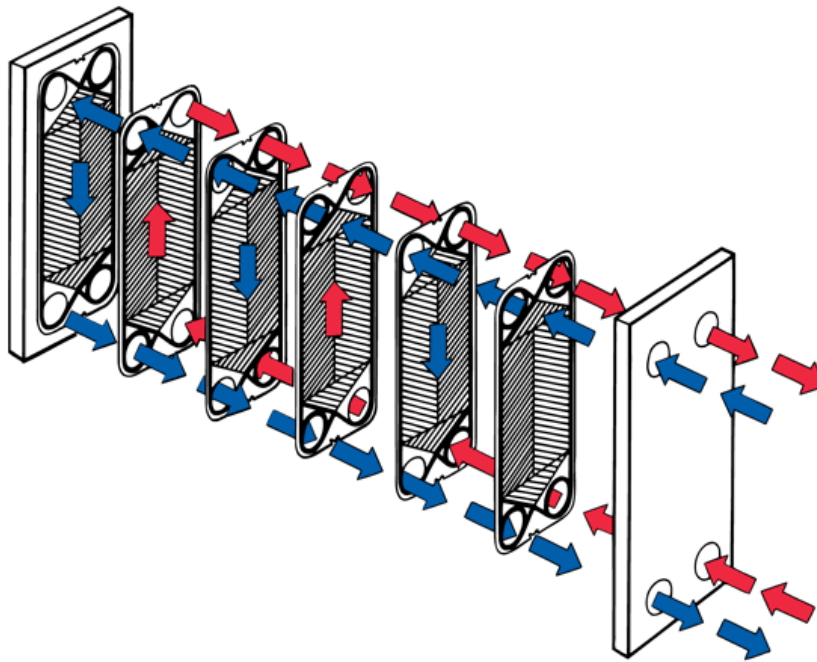
Figure 13 Illustration of a plate heat exchanger (30)

Two streams can be seen in Figure 13, one hot and one cold. On every plate there is a seal preventing the two streams from mixing with each other. In order for these seals to hold, the heat exchanger package needs to be pressed together using bolts and nuts. In Figure 13 certain patterns can be seen on the plates. These patterns are referred to as corrugations. Plate corrugations are used to enhance the heat transfer properties. There are several different types of corrugations. The most common corrugation type is the *chevron* type, but there are also intermating patterns. The chevron corrugation pattern is formed as a "V". The angle of these corrugations can vary from exchanger to exchanger. Normally a larger chevron angle results in higher heat transfer but also higher pressure drops.

The main equation for the heat flow Q between fluids can be written as

$$Q = UA\Delta T_M \qquad\qquad \text{\{Eq. 23\}}$$

where U is the overall heat transfer coefficient. A is the total plate area and ΔT_M is the effective temperature difference. U depends mainly on the heat transfer coefficients of the fluids and the shape of the corrugations. ΔT_M is a function of the stream temperatures, stream heat capacities and the heat exchanger configuration. It is important to consider how the area A should be defined. It can be defined as either the projected surface area of the plates or as the total surface area including the corrugations. Here A refers to the projected surface area of the plates (29).

When evaluating the performance of the heat exchanger the heat transfer coefficient U is given by

$$\frac{1}{U} = \frac{1}{\alpha_h} + \frac{t}{\lambda_p} + \frac{1}{\alpha_c} + R_f \qquad\qquad \text{\{Eq. 24\}}$$

Here α is the heat transfer coefficient of the hot stream and the cold stream respectively, λ_p is the plate conductivity, t is the plate thickness and R_f is a fouling factor. Correlations between the flow conditions and heat transfer properties are shown in Figure 14.
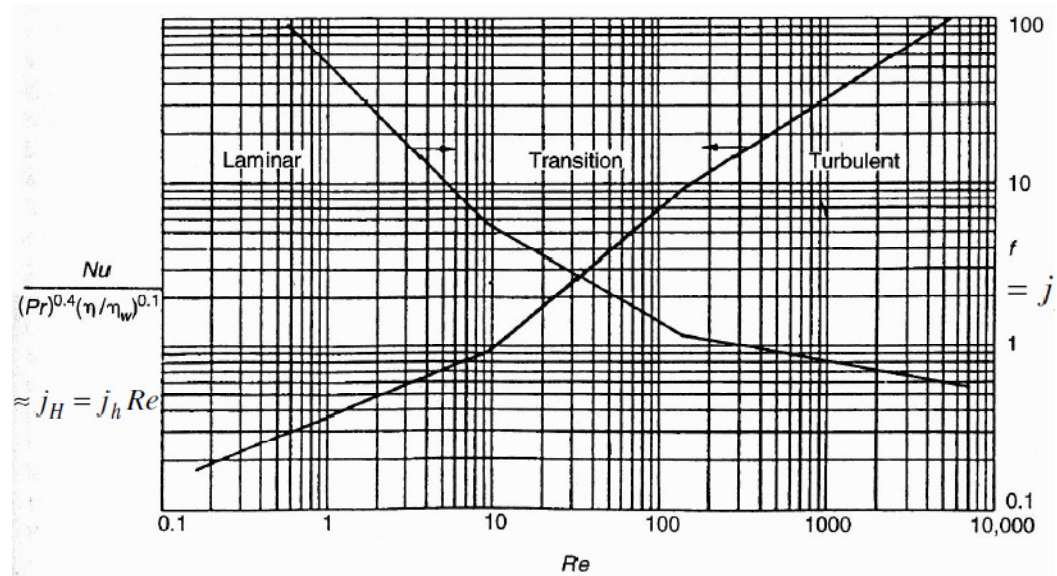
Figure 14 Correlations between Reynolds number and heat transfer properties (29)

The non-dimensional factors in Figure 14, Nu, f, R_e and j_H are defined as

$$Nu = \frac{\alpha D_e}{\lambda} \qquad \text{\{Eq. 25\}}$$

$$f = \frac{\Delta p}{\left(\frac{4L}{D}\right)\left(\frac{\rho u^2}{2}\right)} \qquad \text{\{Eq. 26\}}$$

$$R_e = \frac{\bar{u} D_e \rho}{\mu} \qquad \text{\{Eq. 27\}}$$

$$j_H = j_h Re = \frac{Nu}{Pr^{0.4}\left(\frac{\mu}{\mu_w}\right)^{0.1}} \qquad \text{\{Eq. 28\}}$$

where $\bar{u}$ is the mean flow velocity between the plates and α is the mean heat transfer coefficient between the plate surface and the fluid. Δp is the fractional pressure drop between the ends of the plate of length L. D_e is the equivalent diameter of passage. The fluid properties ρ, η, and λ are calculated at the mean fluid temperature. μ and μ_w are the fluid dynamic viscosity in the bulk and near the wall respectively. The common definition of D_e for plate heat exchangers is

$$D_e = 2b \qquad \text{\{Eq. 29\}}$$

where b is the axial distance between two adjacent plate surfaces. One important factor when designing a plate heat exchanger is the maximum acceptable pressure drop. Increasing the heat transfer properties of the heat exchanger leads to increased pressure drop. This can be seen from Eq. 26 Figure 14where an increased friction factor leads to higher pressure drop. These factors will need to be weighted in order to achieve a compact heat exchanger design without exceeding the acceptable pressure drops.

The heat transfer under free convection conditions across a vertical plate can be estimated using the Rayleigh number (Ra) and empirical correlations for the Nusselt (Nu) number (28). The Rayleigh number is a function of the gravitational acceleration G, the temperature of the surface, T_s, as well as the temperature of the bulk flow, T_∞, the kinematic viscosity ν and the thermal diffusivity σ. For vertical plates the Rayleigh number is given as

$$Ra_x = \frac{G\beta(T_s - T_\infty)x^3}{\nu\sigma} \qquad \text{\{Eq. 30\}}$$

where β is the inverse of the mean fluid temperature in Kelvin and x is the length of the plate.

As suggested by Churchill and Chu (31) the Nusselt number for vertical plates can be calculated using

$$\overline{Nu}_L = \left\{0.825 + \frac{0.387 * Ra_L^{1/6}}{\left[1+\left(\frac{0.492}{Pr}\right)^{9/16}\right]^{8/27}}\right\}^2 \qquad \text{\{Eq. 31\}}$$

3.4.5   Heat exchanger size

A larger upgrading capacity requires more heat transfer surface and therefore larger heat exchangers. As shown by Chang, Chung and Park (27) the accumulation is concentrated to a rather small area, increasing the length of the heat exchanger plates is therefore not of the greatest importance. This is assuming that all (or nearly all) the

CO_2 still has sufficient time to desublimate before reaching the end of the heat exchanger plates, otherwise the length has to be increased.

The plate spacing is typically in the range from 2 to 6 mm and a larger spacing implies a larger area for the biogas to flow through. This reduces the flow velocity compared to the heat transfer surface area, assuming that all other dimensions of the heat exchanger are unchanged. The Reynolds number is unaffected by the plate spacing, since the factors cancel each other out. This would suggest that the turbulence is the same independently of the plate spacing (29).

Increasing the number of plates in the heat exchanger divides the flow into a larger number of streams. This reduces the mass flow rate and flow velocity in each individual stream. This results in a longer residence time and an increased area that the CO_2 comes into contact with. The reduced velocity results in less turbulent flow conditions and reduced heat and mass transfer properties.

4   Experimental setup

This chapter provides a description of the process and describes the purpose and setup of the tests.

4.1   Process description

The test rig consists mainly of two plate heat exchangers, HX A and HX B. HX A is used for the desublimation of CO_2. HX B is used to cool the refrigerant media which in turn cools HX A. N_2 (l) is used to cool the refrigerant media, which is a mixture of LPG and N_2 (g). "g" indicates gaseous phase and "l" indicates liquid phase.

A simplified process schematic of the test rig is shown in Figure 15. Liquid nitrogen is filled in a container connected to HX B. This container is placed on the same level as HX B. There is a certain level of liquid nitrogen filling up HX B, which evaporates continuously under atmospheric pressure. The gas mixture of LPG and N_2 partly condenses into a liquid refrigerant on the opposite side of the heat exchanger. The refrigerant stream enters HX A counter-currently and vaporizes. CO_2 desublimates from the biogas stream while CH_4 is left in gaseous form.
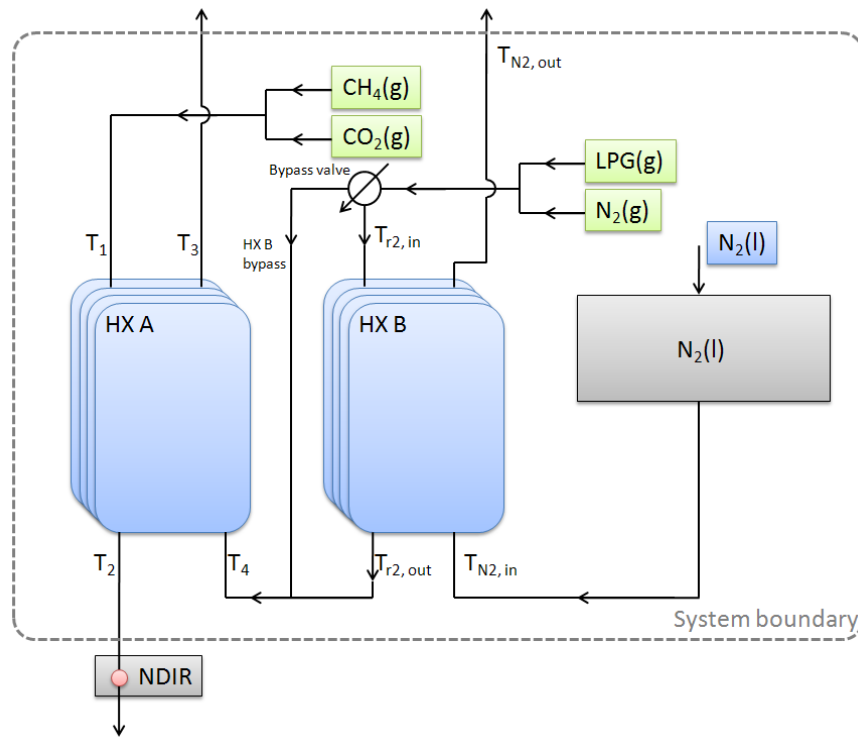
Figure 15 Simplified lab rig schematics

CH_4 and CO_2 are injected into the rig using pressurized canisters, and so are the components of the refrigerant. In order to analyze the gas concentrations in the outgoing biogas a NDIR sensor is used. It analyzes the spectroscopic properties of the gas, i.e. its ability to absorb infra red light with certain wavelengths. A NDIR sensor consists of an infrared lamp directed towards the gas stream. A detector with an optical filter that removes all light except the light with the specific wavelength of

interest is mounted behind the gas stream. The sensor registers the volumetric fraction of the measured specie in the gas stream.

The analyzer uses a gas pre-treatment system to extract 60 liters/hour of biogas from the test rig. When there is no biogas flow through the NDIR sensor, the system analyzes the surrounding air. This explains the registered level of O_2 later when the results are presented.

The two plate heat exchangers used in this experimental setup consist of 10 chevron corrugated plates each. The plates have a width of 72 mm and a height of 187 mm. The heat exchangers are configured as one pass/one pass, i.e. the two streams only pass the plates one time before reaching the outlet. One of the main advantages with the proposed test rig design is that it consists of simple components. The process is designed to run under a relatively low pressure which further reduces the need for expensive components.

In order to measure the temperature distribution across HX A, five thermocouples are attached to the back side of the exchanger. The placement of the thermocouples is illustrated in Figure 16, where the specified dimensions are given in millimeters. The figure is oriented in the same way as shown in Figure 15, with the incoming biogas entering from the top and the refrigerant media entering from the bottom.
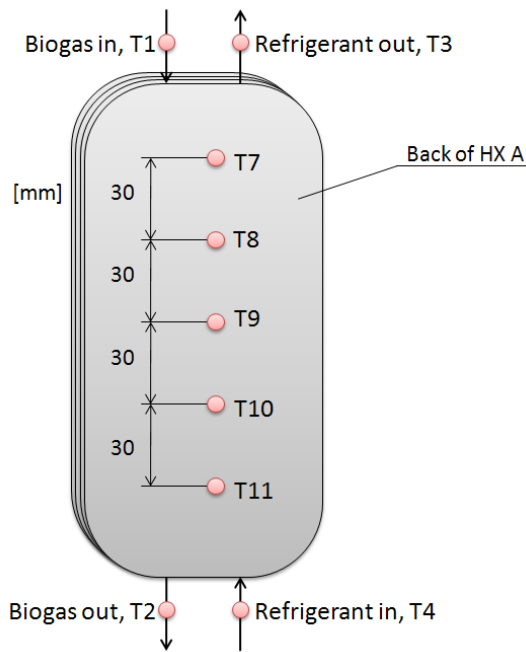
Figure 16 HX A thermocouple placement

It should be mentioned that the refrigerant media flows on the other side of the plate where the thermocouples are placed.

The flow rate is measured using Kytola® A-2BR Flow meters which are calibrated for the flow of air at 20 °C and atmospheric pressure. These conditions are hereafter referred to as "normal" conditions. They can also be used to measure flow rates for other gases using a recalculation formula given by Kytola®. This formula is

$$\dot{V} = \dot{V}_0 \sqrt{\frac{r_1 * T_1 * p_2}{r_2 * T_2 * p_1}}$$
{Eq. 32}

where $\dot{V}$ is the calculated real normal flow rate for the gas flowing through the meter. $\dot{V}_0$ is the displayed value of the Kytola$^®$ A-2BR flow meter. r_1 is the specific gravity of air, r_2 is the specific gravity of the measured gas. T_1 is the normal temperature, i.e. 293 K. T_2 is the temperature of the gas flowing through the meter. p_1 is the normal pressure, 1.013 bar (absolute pressure) and p_2 is the pressure of the gas flowing through the meter.

The time to heat exchanger "freeze-in" where the gas flow is hindered from passing through the heat exchanger was estimated. The volume available for gas flow inside the heat exchangers is approximately 0.00027 m^3. Using the assumption from Chapter 3.3 that the CO_2 frost density is around 500 kg/m^3 and assuming a CO_2 mass flow rate of $7.38*10^{-5}$ kg/s, the time to total "freeze-in" is 4100 seconds, or 68 minutes. The accumulated mass of CO_2 frost is then equal to 135 grams assuming that the frost layer is evenly distributed over the entire heat exchanger surface area.

4.2 Heat balance

In order to get an estimate of the process heat flow requirement a general heat balance over the two heat exchangers is presented here. A linear approximation for the species specific heat values (C_p) is used when calculating the heat removal demand. The notation i refers to the heat of sublimation and the heat of vaporization for the species. The LPG in the refrigerant media completely condenses in HX B and later completely vaporizes in HX A. The liquid nitrogen completely vaporizes in HX B. For the desublimation efficiency, η_d is used. It represents the mass flow of desublimated CO_2 in relation to the incoming CO_2 mass flow.

In this analysis, heat transfer with surroundings is neglected. The actual heat losses were measured, and are presented in Chapter 5.2.

Heat exchanger A

Figure 17 shows a schematic illustration of the heat transfer and CO_2 accumulation on one plate in HX A. The heat is transported from the hot biogas stream across the plate to the cold refrigerant stream.
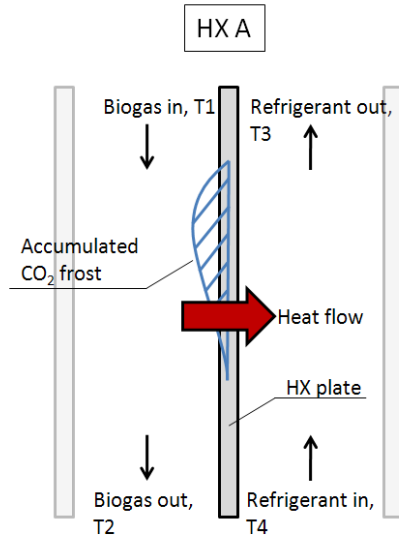
Figure 17 Schematic overview of one plate in HX A

$$\dot{Q}_{bg} = \dot{m}_{CH4} \int_{T_1}^{T_2} Cp_{CH4} dT + \dot{m}_{CO2} \int_{T_1}^{T_2} Cp_{CO2} dT - \eta_d \dot{m}_{CO2} i_{CO2} \qquad \{Eq.\ 33\}$$

$$\dot{Q}_{r1} = \dot{m}_{LPG} \int_{T_4}^{T_3} Cp_{LPG} dT + \dot{m}_{N2} \int_{T_4}^{T_3} Cp_{N2} dT + \qquad \{Eq.\ 34\}$$
$$\dot{m}_{LPG} i_{LPG}$$

$$\dot{Q}_{bg} + \dot{Q}_{r1} = 0 \qquad \{Eq.\ 35\}$$

Heat exchanger B

The other heat exchanger in the system, HX B, is shown in Figure 18. Heat is transferred from the hot refrigerant stream to the liquid nitrogen, which evaporates.
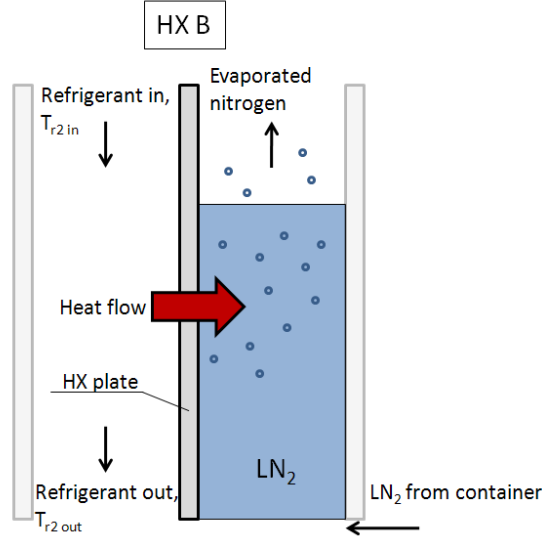
Figure 18 Schematic overview of one plate in HX B

$$\dot{Q}_{r2} = \dot{m}_{LPG} \int_{T_{r2\,in}}^{T_{r2\,out}} Cp_{LPG} dT + \dot{m}_{N2} \int_{T_{r2\,in}}^{T_{r2\,out}} Cp_{N2} dT - \dot{m}_{LPG} i_{LPG} \qquad \text{\{Eq. 36\}}$$

$$\dot{Q}_{N2_l} = \dot{m}_{N2_l} \int_{T_{N2\,in}}^{T_{N2\,out}} Cp_{N2_l} dT + \dot{m}_{N2_l} i_{N2} \qquad \text{\{Eq. 37\}}$$

$$\dot{Q}_{r2} + \dot{Q}_{N2_l} = 0 \qquad \text{\{Eq. 38\}}$$

The required heat removal from the primary biogas stream in order to desublimate all the CO_2 is 580.9 kJ/m$_n^3$ biogas. The incoming biogas has a temperature of 20 °C and an exit temperature of -90 °C. The biogas consists of 40% Vol. CO_2 and 60% Vol. CH_4. The amount of required heat removal can be compared to the calorific value of the biogas when combusted with oxygen i.e.

$$\Delta Hc_{CH4} = 50.216 \frac{MJ}{kg\ CH4} \qquad \text{\{Eq. 39\}}$$

$$Y_{CH4} = 0.6 \frac{mol\ CH4}{mol\ biogas} * \frac{0.016\ kgCH4/mole\ CH4}{0.0272\ kg\ biogas/mole\ biogas} = 0.353 \frac{kg\ CH4}{kg\ biogas} \qquad \text{\{Eq. 40\}}$$

$$\Delta Hc_{biogas} = \Delta Hc_{CH4} * Y_{CH4} = 17.73 \frac{MJ}{kg\ biogas} = 21.52 \frac{MJ}{m_n^3\ biogas} \qquad \text{\{Eq. 41\}}$$

The biogas heat removal demand amounts to 2.7% of the calorific value of the biogas. The heat flow needed to cool the incoming biogas stream from 20 to around -90 °C and desublimate all the CO_2 is 50 W. This is calculated using flow rates for CH_4 and CO_2 of 1.23 and 0.82 l/min respectively at a pressure of 3 bar. In order to keep the temperature inside HX A constant, the refrigerant media has to transport this heat away. One important fact about the separation process is that 84% of the heat removal demand comes from the CO_2 desublimation heat.

The convective heat transfer coefficient for the refrigerant flow inside HX B is 70 Wm^{-2}K^{-1} using the theory in Chapter 3.4.4. The flow rates of the refrigerants are

2.78 l/min and 1.85 l/min for LPG and N_2 respectively. These flow rates are specified for an operational pressure of 2 bar. For simplicity, effects from the condensation of the refrigerant media are not included in these calculations. The condensation leads to increased heat transfer properties of the refrigerant flow. The heat transfer is dependent on the gas flow rates, where a higher gas flow rate results in an increased convective heat transfer coefficient.

The heat transfer on the liquid N_2-side of HX B is regarded as free convection heat transfer across a vertical plate. Using the correlations for Ra and Nu in Eq. 30 and Eq. 31 the convective heat transfer coefficient is 282 $Wm^{-2}K^{-1}$. The total heat transfer coefficient U, given by Eq. 24 is dominated by the heat transfer on the limiting side of the heat exchanger. In this case the convective heat transfer coefficient is much larger on the liquid N_2 side. The total heat transfer is limited by the refrigerant flow and not by the liquid N_2. The value of the overall heat transfer coefficient U is then 56 $Wm^{-2}K^{-1}$. The impact of the heat transfer resistance from the heat exchanger material (steel) is neglected.

4.3   Purpose of tests

The tests were conducted in order to answer a certain set of questions regarding the heat exchangers ability to separate CO_2 from CH_4. The main questions to be answered were

1. Can biogas with less than 1% Vol. CO_2 be produced during at least 5 minutes of operation?
2. What operational parameters affect the heat exchanger functionality?
3. What characterizes the regeneration process? How long time is required?

Other questions connected to the main questions:

- How is the biogas purity, i.e. the outlet volumetric concentration of methane, affected by the heat exchanger surface temperature?
- What effect on the frost formation has an increased mass flow rate of incoming biogas?
- Will there be any unforeseen complications due to the frost formation?

4.4   Procedure

Before the start of the separation process the incoming biogas composition was adjusted to resemble a typical composition of biogas, i.e. 60% Vol. CH_4 and 40% Vol. CO_2. The volumetric flow rate of the biogas as well as the operational pressure was set prior to the start of the "cool-down" process. Liquid nitrogen was filled into the container in order to cool down HX B. The refrigerant media was then used to cool down HX A prior to starting the separation cycle.

The critical temperature for the initial CO_2 desublimation is around -80 °C under pressurized conditions, see "sublimation line" in Figure 8. Once HX A had reached a sufficiently low temperature, the refrigerant media was adjusted to an adequate mass flow rate and temperature needed to transfer all required heat from the biogas. After this the biogas flow was started and the desublimation of CO_2 started instantly. The separation process continued until the differential pressure over HX A became too large, or until the outlet concentration of CO_2 became too high.

After the separation process had finished and HX A had frozen up with CO_2, the heat exchanger was regenerated. This was done by letting the refrigerant media pass through HX A without first being chilled in HX B. This was possible by changing the setting of the bypass valve which can be seen above HX B in Figure 15, diverting the flow from the heat exchanger. When the regeneration process was started, the temperature inside HX A was still below the desublimation temperature of CO_2 and the temperature first had to be increased to a point where sublimation of CO_2 could start. Once HX A reached a high enough temperature, the CO_2 frost was sublimated to gas and was pushed out of the system. The extracted CO_2 could be captured if desirable. This regenerative process continued until all the frozen CO_2 had been sublimated. After this, HX A was ready for the next separation cycle.

5 Results and discussion

In this chapter, results regarding the operation of the test rig as well as the results from gas composition measurements and temperature measurements are shown. The separation chapter is divided into several different test scenarios with different initial and operational parameters which are documented in Table 5. Following the results from each test are some discussions regarding different aspects of the separation process. All gas concentrations are given as volumetric fractions.

5.1 Experimental experiences

Due to the fact that the density of the gas increases when the temperature is lowered as well as that the incoming CO_2 is being desublimated, the pressure was not the same during operation as it was prior to cool-down. Therefore it was problematic to test the CO_2 separation process under specific controlled pressures. The biogas flow rate increased compared to the pre-set values as a result of the lowered pressure inside the test rig.

At temperatures approaching -196 °C, LPG becomes highly viscous. This resulted in that HX B "clogged" up with LPG, which had negative impact on the heat transfer properties of the refrigerant. After a certain amount of time it became impossible for the refrigerant flow to pass through HX B. The LPG was instead switched to methane with a purity of around 99.7% methane. Included in the 0.3% of remaining substances are mainly other hydrocarbons and around 5 ppm of water. Improvements to the heat transfer properties were noticed compared to when using LPG. The problem with the "clogging" up of HX B did however not disappear completely.

Relative to the flow rates of gas passing through the two heat exchangers, the thermal inertia of the heat exchangers was very large. The thermal inertia of an object refers to the amount of heat required to change its temperature. Achieving a uniform temperature distribution in HX A was shown to be difficult, especially during tests with low heat exchanger temperatures, i.e. below -100 °C. During these tests the average temperature over all the measuring points on the heat exchanger was used to determine the starting temperature conditions. These conditions were not ideal to draw conclusions from, since the temperature difference over the heat exchanger was large. As a matter of fact, the distribution of the frost layer across the heat exchanger surface as well as the density of the frost layer varied along the heat exchanger.

5.2 Separation

The biogas purity, i.e. the volumetric outlet concentration of CH_4 in the upgraded gas was the main parameter of interest during the tests. The time for one separation cycle to complete, i.e. the time until the "freeze-in" of HX A, was in the range of 10 minutes assuming that the flow rate of CO_2 was kept according to the value specified in Chapter 4.2.

In Table 5 the different operating conditions during the separation tests are shown. As can be seen from Table 5, the values measured during operation differ quite a bit between the different tests. This is due to that the flow rate, pressure and temperature depend on each other. The average temperature specified is the average temperature of HX A prior to start.

Table 5 Test operating conditions

Test	Inlet CO_2 concentration [%] [1]	$\dot{V}_{CO2}$[l_n/min] [2]	$\dot{V}_{CH4}$[l_n/min] [2]	Absolute pressure [bar] [2]	Average temperature HX A [°C] [1]
1	37.2	1.13	1.88	1.8	-122
2	38.3	1.08	2.06	2.0	-111
3	37.9	2.07	3.40	2.0	-111
4	37.4	1.21	1.93	1.0	-111
5	38.0	1.13	1.88	1.8	-82
6	38.2	1.14	2.08	2.0	-92
7	37.8	0.91	2.06	2.0	-102
8	37.8	1.10	2.10	1.7	-110

As can be seen in Table 5 the ratio between the volumetric flow rates of CO_2 and CH_4 does not exactly equal the inlet CO_2 concentration specified. This was due to that the flow meters were read manually, where some measurement uncertainties were incorporated. The concentrations given by the digital NDIR-sensors were used determine the inlet CO_2 concentrations.

A summation of the biogas purity as a result of different temperature in HX A during the tests is shown in Table 6. The biogas purity for Test 1-4 was registered during the initial period of the tests, before the purity had started to decrease because of increasing temperature in HX A. The presented biogas purity for Test 5-8 was taken as an average value during the separation period.

---

[1] Measured values prior to biogas separation
[2] Measured values during biogas separation

Table 6 Biogas purity as result of HX A temperature

Test	HX A Temperature [°C]	Biogas purity [%]
1	-122	100
2	-111	100
3	-111	99
4	-111	99
5	-82	84
6	-92	98
7	-102	99.5
8	-110	100

Figure 19 shows the measured volumetric concentration of CO_2 and the theoretical saturation curve for CO_2 as a function of heat exchanger temperature. The measured concentrations are below the values for what is theoretically possible to reach. This is due to that the measured values are given for the average temperature of HX A. The temperature was however lower in the bottom part of the heat exchanger, which explains the lower concentrations.
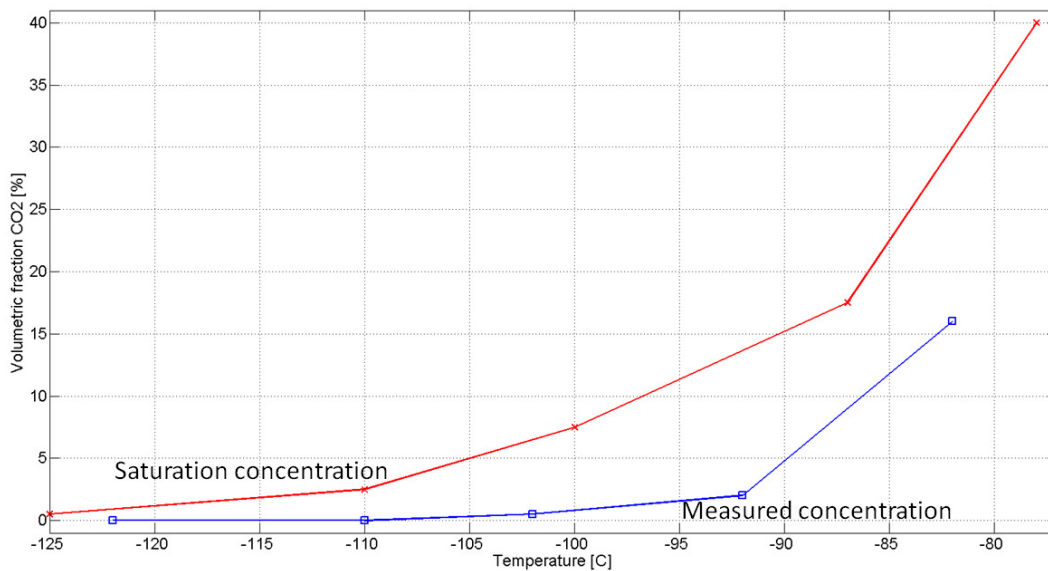
Figure 19 Measured and saturated volumetric CO_2 concentration

The accumulated amount of CO_2 in the heat exchanger was calculated by integrating the NDIR measurements over the separation period. The inlet volumetric concentration of CO_2 prior to start was known. By subtracting the known incoming CO_2 concentration with the value measured by the NDIR sensor and using the incoming mass flow rate of CO_2, an estimate of the mass accumulation was obtained. The results from these calculations are shown in Table 7.

Table 7 Accumulated amount of CO2

Test	Accumulated CO_2 [g]	Accumulated CO_2 per heat transfer surface [g/m^2]	Stopping condition
1	23.8 (13.3 [3])	238.5 (133.3 3)	Low biogas purity
2	26.6 (13.6 3)	266.6 (136.3 3)	HX A freeze up
3	31.0 (13.6 3)	310.6 (136.3 3)	Low biogas purity
4	18.6 (11.3 3)	186.4 (113.2 3)	Low biogas purity
5	10.1	101.2	HX A freeze up
6	18.2	182.4	HX A freeze up
7	15.9	159.3	HX A freeze up
8	15.7	157.3	HX A freeze up

The calculated amount of CO_2 that could be desublimated inside the heat exchanger, as stated in Chapter 4.1, was 135 g. This was shown to differ greatly from the results of the test runs, as did the freeze in time discussed in the same chapter. During the experimental tests between 10.1 and 31.0 grams of CO_2 was desublimated. The projected heat transfer surface of the heat exchanger was 0.1 m^2.

Before the biogas flow was started there were significant heat losses to the surrounding, or to be correct heat losses to the test rig. The refrigerant media mass flow rate combined with the inlet and outlet temperature needed to keep the temperature of HX A constant gave an indication about the heat losses. In "standby"-mode before initiating biogas flow, the heat exchange with the surrounding amounted to 11 W. This was calculated from the data registered during Test 3. The resulting refrigerant conditions were found to be 9.8 l$_n$/min with an inlet temperature close to -130 ℃.

In the presented tests the temperature required to reach concentrations below 2% CO_2 is marked with a dashed line. This is the saturation temperature of CO_2 at the corresponding partial pressure for 2% CO_2 corresponding at 2 bar to the desired purity of 98% methane. The saturation temperature however varies with CO_2 concentration and total pressure.

---

[3] These values are the amount of captured CO_2 during operation with at least 98% volumetric outlet concentration of CH_4

5.2.1 Test 1

Constant inlet temperature and mass flow of the refrigerant media was used to establish the distribution of the heat flow inside HX A. The resulting NDIR measurements are shown in Figure 20. The biogas flow was initiated about 50 seconds into the plot timeline, where a sharp increase in the amount of CH_4 can be seen. Since the aim of the test was to determine the heat flow and temperature flux caused by the incoming biogas, the temperature of the heat exchanger was allowed to increase and the outlet biogas purity to be low.
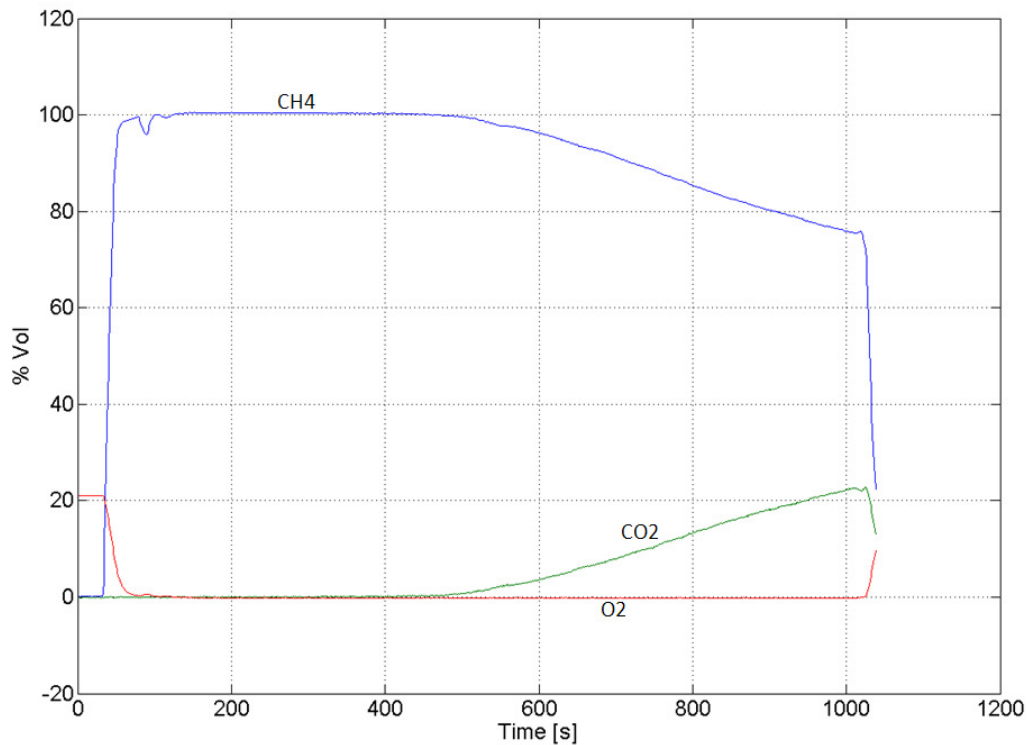
Figure 20 NDIR measurements, Test 1

The outlet CH_4 concentration stabilized at around 100% after a few seconds of operation. This level of biogas purity was maintained until about 500 seconds into the test, when the outlet CH_4 concentration started to decrease.

The corresponding temperature distribution along the heat exchanger is shown in Figure 21. There was a steady temperature increase all along HX A after the biogas flow was started, 50 seconds into the graph. Before that, the slight increase of the temperatures was due to heat losses. Initially after the biogas flow was started, the largest temperature increase was at measuring Point 7. This point was also the one closest to the biogas inlet. The temperature at the points further downstream of HX A increased one after another. After about 250 seconds the increase rate of T7 slowed down, approaching a level similar to the one prior to the start of the biogas flow.

The desublimation temperature corresponding to a concentration of 2% CO_2 is as previously mentioned also plotted. It can be noted that when this temperature intersected T11 the biogas purity started to decrease as shown in Figure 20.
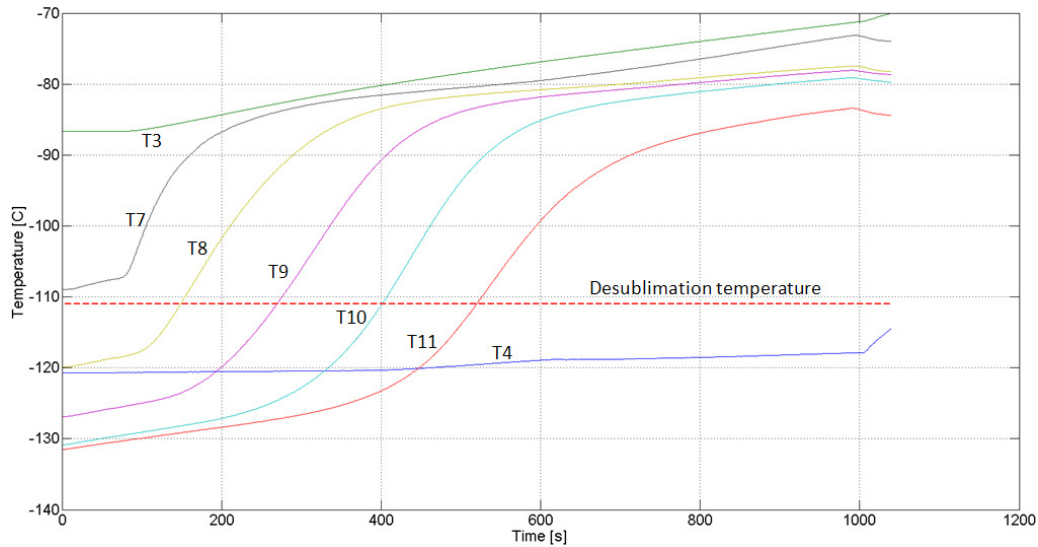
Figure 21 HX A temperature distribution, Test 1

By differentiating the temperature change over time at the different measurement points in Figure 21, and by knowing the thermal inertia of the heat exchanger, the heat flow at the different points for a specific time was calculated. The total heat flow is the sum of the independent points with an area of 0.018 m^2 each. It should be noted that the "Heat Flow" plotted in Figure 22 originates from the temperature derivative with respect to time in HX A, and a low plotted heat flow does not necessarily mean that no heat is flowing from the biogas to the heat exchanger surface. The large initial changes in the temperatures were due to that the heat exchanger temperature was not in equilibrium with the heat from the incoming biogas. As the temperature profile leveled out, the heat flow decreased towards zero, and the system approached a stable operating point.

There was a close correlation between the total heat flow and the biogas purity, shown in Figure 22 and Figure 20. After 500 seconds the total heat flow decreased drastically. At the same time the outlet concentration of CH$_4$ started to decrease.
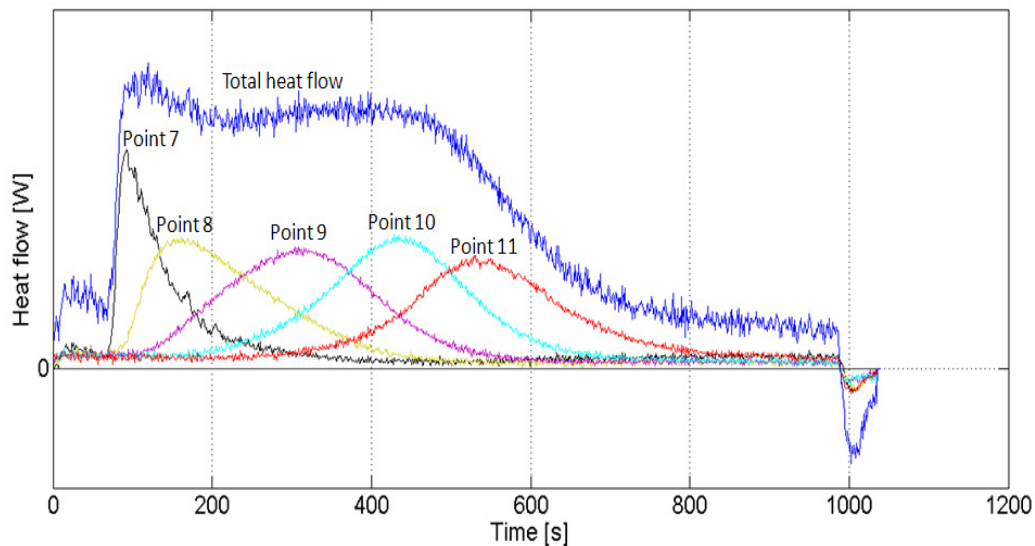
Figure 22 HX A heat flow, Test 1

The largest heat flow after the start of the biogas flow was located at Point 7. After around 130 seconds the largest part of the heat flow was at Point 8 while the heat flow at Point 7 steadily decreased towards zero. This trend followed throughout the separation process, where the point downstream of the previous one increased as the heat flow at the point upstream decreased. After 800 seconds the temperature gradients in Figure 21 leveled out and there were no heat flow at the measuring points besides the heat losses.

It can be noted that even though the heat flow at Point 7 was almost zero after 350 seconds, the process was still able to continue without the heat exchanger freezing up and blocking all biogas flow. This means that the CO_2 accumulated at the leading edge was not enough to block the biogas flow.

The accumulated amount of CO_2 inside HX A in this test was calculated to 23.8 grams. As the heat exchanger did not freeze up during the test, the process was instead stopped when the outlet concentration of CO_2 reached about 22%.

5.2.1.1 Discussion

As mentioned in Chapter 4.2 the heat demand from the separation process consists to 84% of the CO_2 desublimation heat. When HX A reached a temperature above the desublimation temperature, a lesser amount of CO_2 could desublimate and a large decrease in heat flow was visible. The heat flow peak after 60 seconds at Point 7 in Figure 22 shows that the main part of the biogas cooling and CO_2 desublimation took place there.

As the CO_2 frost layer was building up at Point 7, the heat transfer surface at that location became more insulated from the biogas flow and the temperature increase at that position was reduced. The heat front gradually advanced downstream of HX A, building up a frost layer along the heat exchanger surface. According to Chang, Chung and Park (27) the CO_2 frost starts to form at a "frost point" and propagates further into the heat exchanger. This propagation behavior correlates well to the results presented here.

After 800 seconds almost no heat flow can be seen from Figure 22 even though there was still CO_2 accumulated according to the NDIR measurements in Figure 20. At this point the outlet biogas purity was 87%. The reason for this low biogas purity was the increased frost layer on the heat exchanger surface, which limited the heat transport from the biogas. The process was here approaching a stable operating point with more constant temperature distribution and CO_2 desublimation efficiency inside the heat exchanger.

5.2.2 Test 2

Test 2, 3 and 4 investigated the internal temperature profile of HX A with different operating conditions for the biogas. A constant mass flow rate and inlet temperature of the refrigerant media was used during these three tests. The mass flow rate was set to 9.8 l_n/min with an inlet temperature close to -130 °C. As mentioned earlier these specific refrigerant flow conditions were used to compensate for the heat losses prior to separation. During the separation process only N_2 was used as refrigerant media. This was done since the CH_4 was connected to both the refrigerant stream and the biogas stream through a "T"-connection. Using the CH_4 for both streams simultaneously would have interfered with the pre-adjusted biogas concentration.

The position of the thermocouples on HX A was changed in this test. They were placed on the side of the heat exchanger instead of on the back. This alteration was done in order to get the thermocouples closer to the biogas stream, as compared to before where they were placed just outside the refrigerant stream. The new thermocouple placement is illustrated in Figure 23.
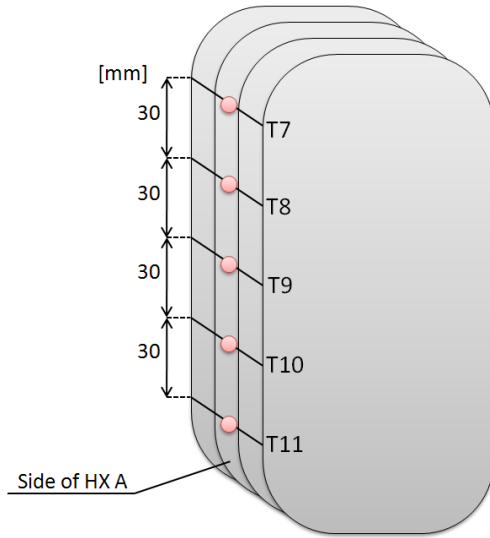
Figure 23 New thermocouple placement

The NDIR measurements are presented in Figure 24. Between 10 and 60 seconds from the initiation of the test, the flow of CH_4 from the rig was step by step replacing the intake of air. The biogas purity was approximately 100% from this point until t = 400 seconds. From there on, the purity gradually decreased. Towards the end, at t = 1000 to 1100 seconds the purity was about 73%.
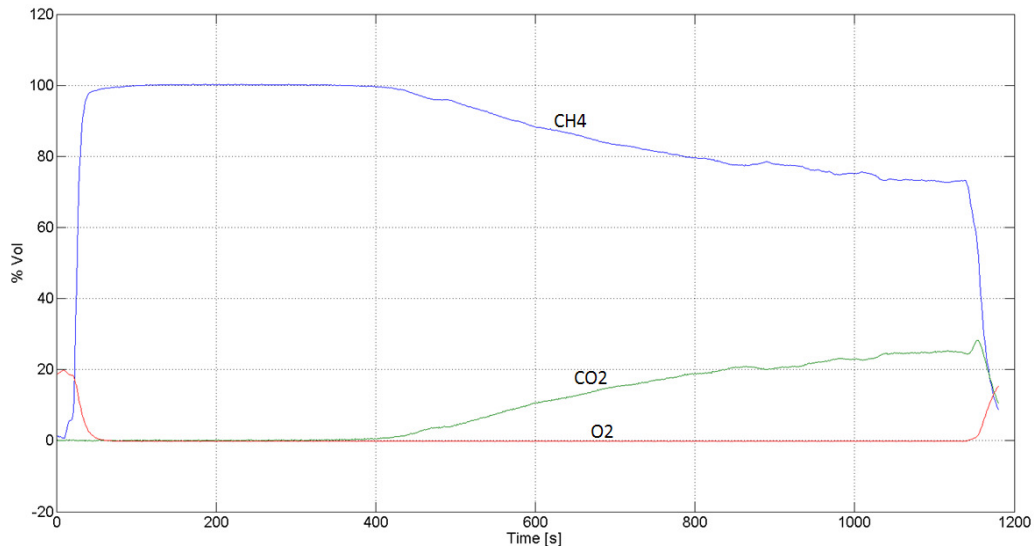
Figure 24 NDIR measurements, Test 2

The registered temperature profiles are shown in Figure 25. The average temperature at the start of the test run was -111.6 °C. The temperature of the incoming refrigerant T4 was kept at -129.5 °C. T7 increased rapidly at first (from 10 to 100 seconds).

42

Thereafter the rate of temperature increase slowed down to a more constant level for the rest of the run. This was due to the increasing CO_2 frost layer and the increasing heat exchanger temperature at that position. T8 to T11 increased in a similar fashion.
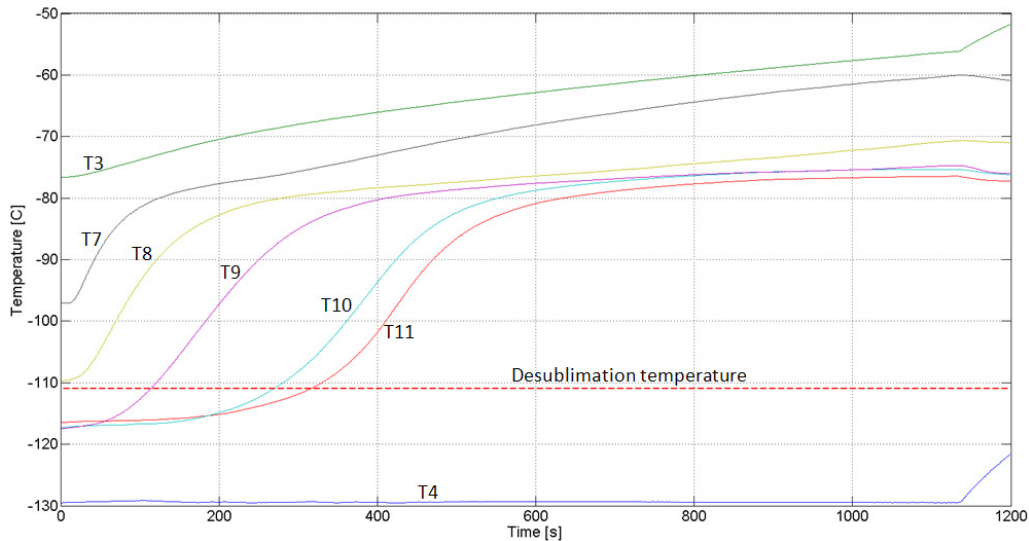
Figure 25 HX A temperature distribution, Test 2

Figure 26 displays the heat flow at Point 7 to 11. The heat flow peak for Point 10 was shifted in time compared to Test 1. This was due to the alteration of the thermocouple placements. After 400 seconds the biogas purity started to decrease, and at that time the heat front had partially passed Point 10 and was almost at its peak for Point 11.
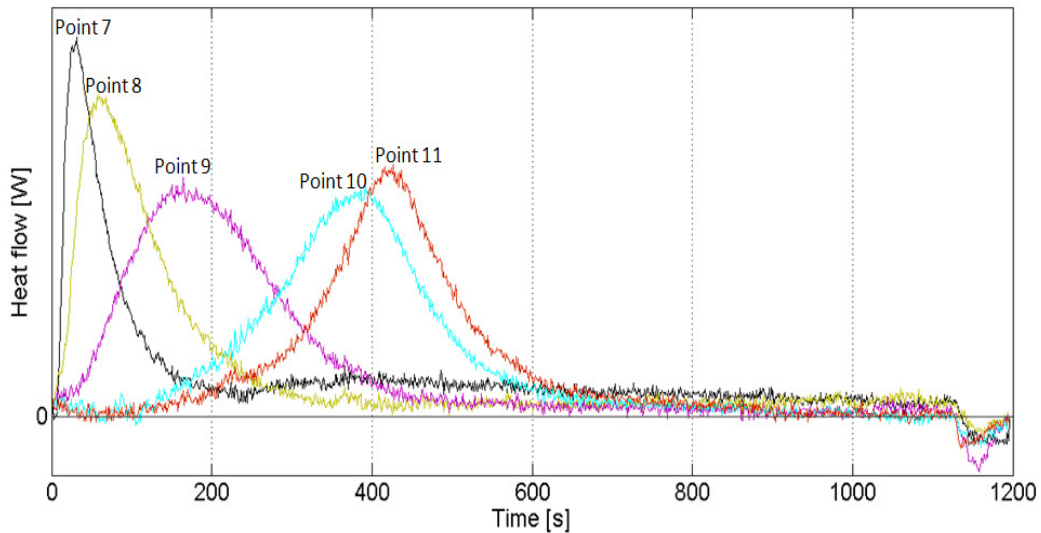
Figure 26 HX A heat flow, Test 2

The pressure inside HX A is shown in Figure 27. Just before the biogas flow was started the pressure was around 1 bar and increased to 2 bar directly after that. The pressure remained constant at 2 bar for 400 seconds. After that point the pressure increased linearly to a peak level of 2.7 bar. At the time 1130 seconds HX A froze up and the biogas flow was stopped. The small peaks along the line were due to

measurement noise from the pressure sensor. The total amount of accumulated CO_2 during this test was 26.6 grams.
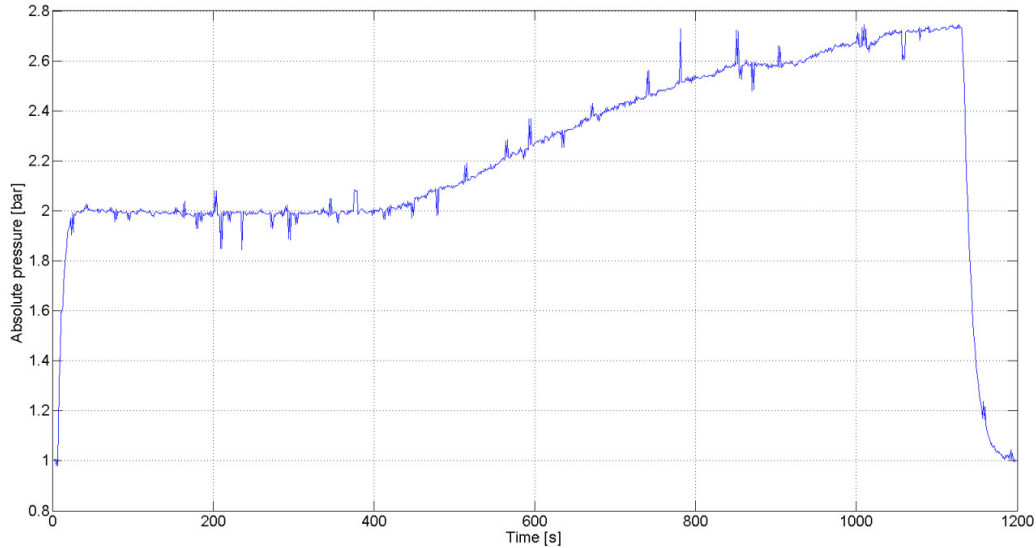
Figure 27 HX A pressure, Test 2

5.2.2.1 Discussion

Apart from the average temperature of HX A, the placement of the thermocouples differed in Test 1 and Test 2. The thermocouple at Point 10 got misplaced during the position change, shifting it too far down HX A. This can be seen from the heat flow at Point 10 in Figure 26, which has moved further to the right. Due to this the total heat flow like the one plotted in Figure 22 for Test 1 was not plotted in Figure 26 for Test 2.

The biogas purity was almost 100% for both Test 1 and 2. The separated amount of CO_2 during Test 1 and 2 was 23.8 and 26.6 grams respectively. The amounts accumulated during the high purity regions were even more similar; 13.3 and 13.6 grams respectively.

The pressure started to increase after 400 seconds during Test 2, which can be seen in Figure 27. This can be explained by looking at the results from the NDIR measurements in Figure 24 where the amount of outgoing CO_2 also started to increase. Since there was then a larger amount of moles gas inside HX A, the pressure increased.

When the total pressure inside the heat exchanger increased as a result of less CO_2 desublimation, it followed that the partial pressure of the CO_2 also increased. This resulted in an increased desublimation temperature of CO_2, which in turn resulted in more desublimation. The system reached an equilibrium point between these factors.

5.2.3 Test 3

Test 3 had same initial settings as Test 2 except that the biogas flow rate was doubled. In Figure 28 the results from the NDIR measurements are shown. The CH_4 concentration was almost constant at 98.9% until about 220 seconds into the test. After this point the output concentration of CH_4 decreased and approached a steady level. The test was stopped after 780 seconds due to low biogas purity. The same thermocouple placement as in Test 2 was used during this test.

44

The accumulated amount of CO_2 during Test 2 and 3 was 13.6 grams and the high purity time periods were 400 and 190 seconds, respectively. The amount of upgraded biogas during the high purity time period was similar in Test 2 and Test 3. The halved time for upgrading the same amount of biogas followed from the doubled biogas mass flow compared to Test 2.
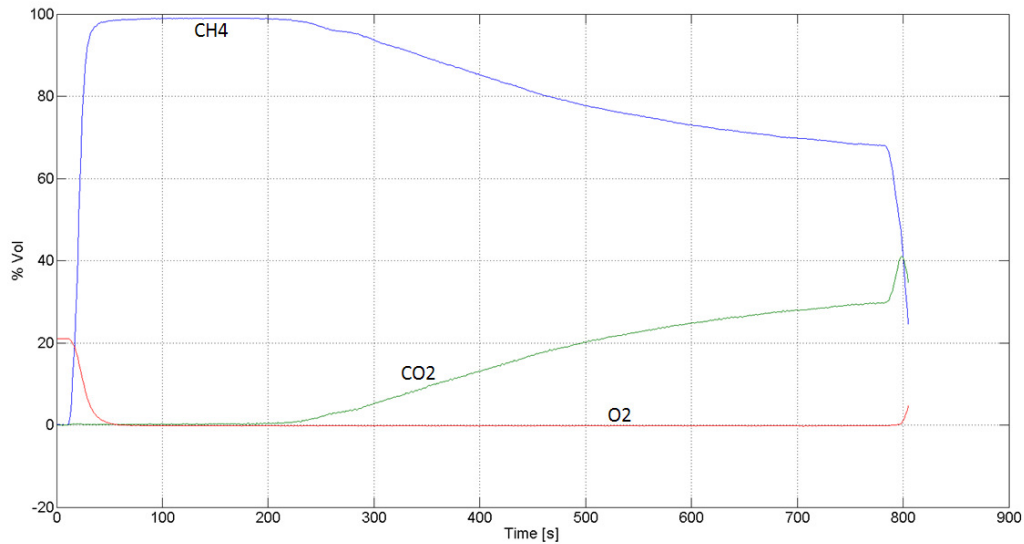
Figure 28 NDIR measurements, Test 3

The temperature distribution inside HX A is shown in Figure 29. The temperature profiles were very similar to the ones in Test 2. The temperatures at the points closest to the biogas inlet increased first, followed by the ones further down.
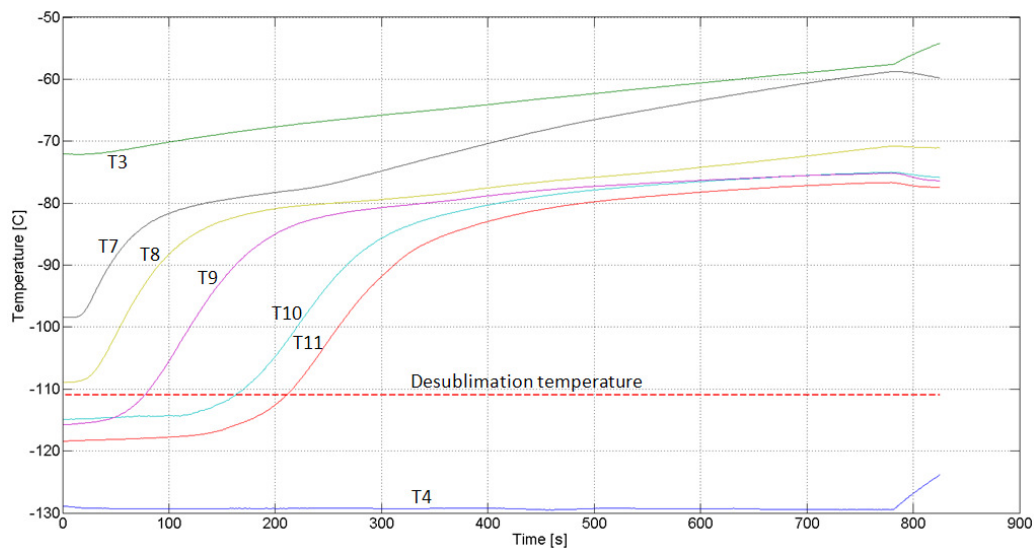
Figure 29 HX A temperature distribution, Test 3

Figure 30 shows the heat flow distribution. The registered values from the thermocouple at Point 10 were irregular with some distinctive fluctuations that were not present at the other measurement points.
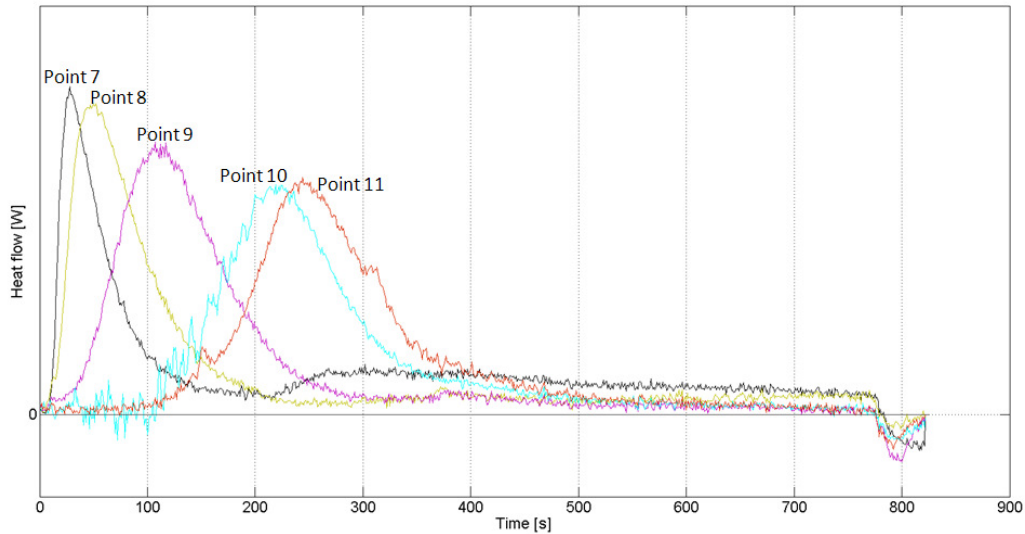
Figure 30 HX A heat flow, Test 3

Comparing the results in Figure 30 with the results from Test 2 in Figure 26 some differences can be noticed. In this test, Point 9 had a higher heat flow for a shorter period of time than Test 2. It also reached its peak point after 110 seconds compared to after 170 seconds in Test 2. Point 10 and 11 peaked earlier and the heat flow was concentrated to a shorter period of time.

5.2.3.1 Discussion

Compared to Test 2, Test 3 had

- Doubled biogas mass flow rate
- Doubled biogas flow velocity
- Halved biogas residence time
- Equal biogas pressure
- Equal HX A temperature

The heat flow in Test 3 was more evenly distributed than in Test 2, with heat peaks more similar in size. This was due to the increased flow velocity, where the residence time in Test 3 was insufficient for the CO_2 to desublimate at the leading edge. The concentration of CO_2 was therefore higher further into the heat exchanger, which increased the heat flow there. As said before, the CO_2 desublimation process represents 84% of the total heat demand. Thus, large differences in heat flow give an indication about this process.

Slightly lower biogas purity was registered during this test, which was due to insufficient residence time. When the biogas flow velocity was doubled, the residence time was halved and the mass transfer coefficient increased by a factor 1.4 $\left(\sqrt{2}\right)$, from Eq. 22. The CO_2 mass transfer rate is given by integrating Eq. 6 over the heat exchanger length. By multiplying the mass transfer rate with the residence time, the amount of separated CO_2 is given. A halved residence time changes the separated amount of CO2 with a factor 0.7 $\left(\frac{1}{\sqrt{2}}\right)$.

46

5.2.4 Test 4

Test 4 investigated the effects of a lower biogas pressure. Figure 31 shows the gas composition measurements from the NDIR gas analyzer. Upon test initiation, the biogas purity reached 98% after 42 seconds. Thereafter the purity remained constant, but increased somewhat towards the max notation 99.4% at t=216 seconds. From there on the purity decreased slowly and at t=290 seconds the purity dropped below 99%. After this point the biogas purity decreased at a steady pace. The same thermocouple placement as in Test 2 was used during this test.

The accumulated amount of CO_2 during the period of high purity (>98% CH_4) was 11.3 grams in Test 4 and 13.6 grams in Test 2. The use of atmospheric pressure shortened the time with high biogas purity to 288 seconds as compared to 400 seconds in Test 2.
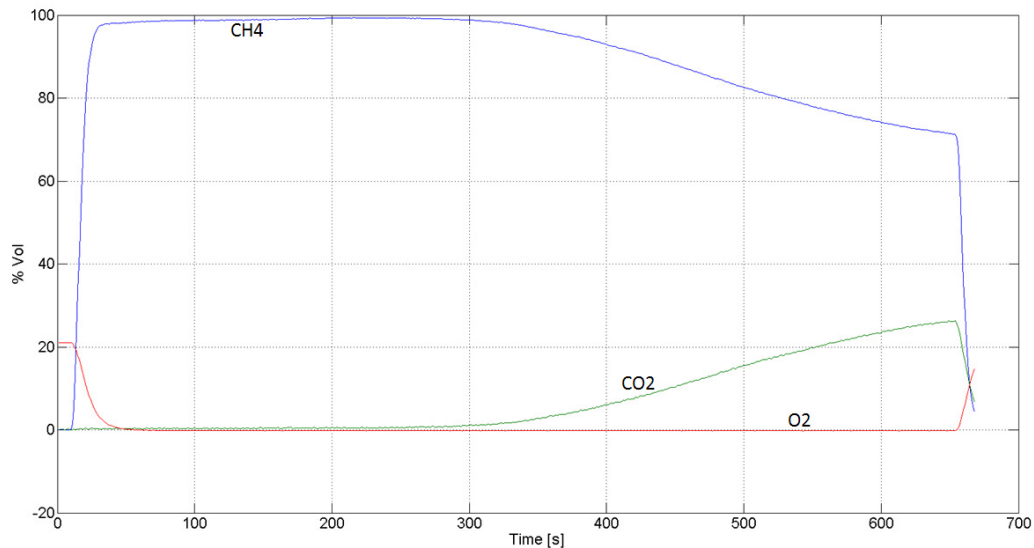
Figure 31 NDIR measurements, Test 4

Figure 32 shows the temperature distribution in HX A and the temperature of the incoming and outgoing refrigerant. The temperature of the incoming refrigerant remained between -131 and -131.5 °C throughout the run. The temperature profiles were similar to those in Test 3, but the rate of temperature decrease for T7 to T11 was lower. This resulted in a less "steep" look of the temperature curves.
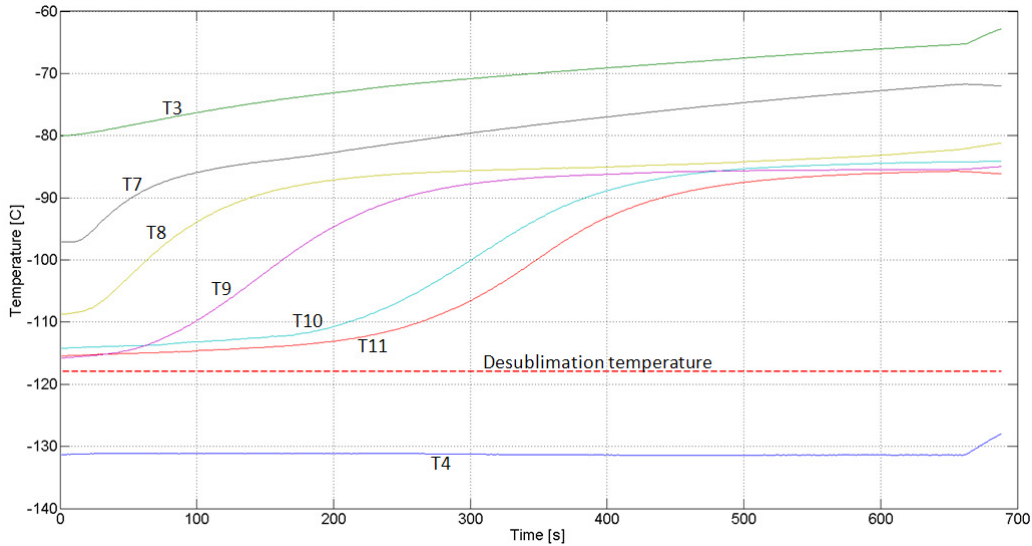
Figure 32 HX A temperature distribution, Test 4

The values from Point 10 were scattered due to measurement noise. The data was therefore time averaged before being plotted.
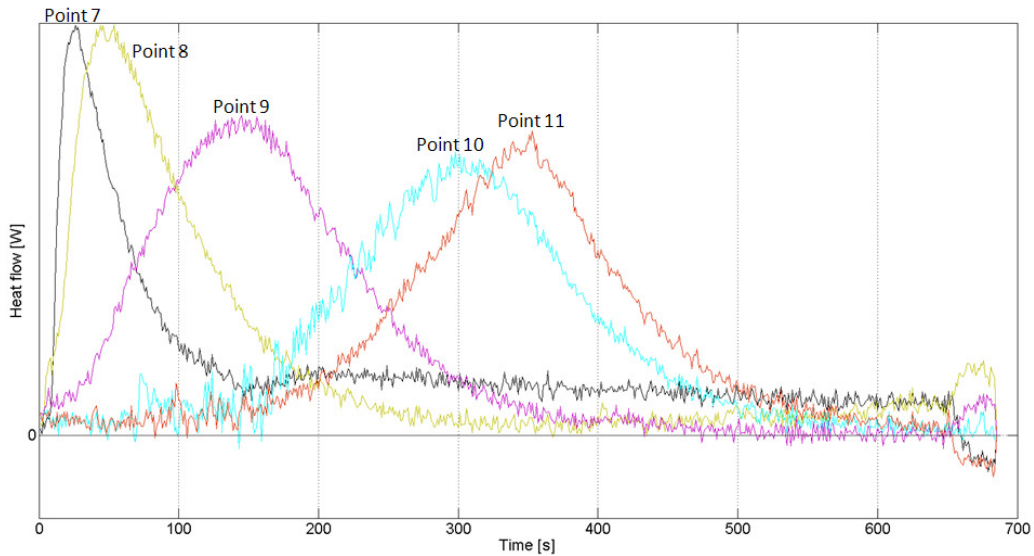
Figure 33 HX A heat flow, Test 4

Point 7-11 had their maximum heat flow earlier in Test 4 than in Test 2. Compared to Test 3, Point 7-8 peaked at the same time while Point 9-11 peaked considerably later in Test 4. When the biogas purity started to decrease after about 300 seconds there was a heat flow peak for Point 10 and the heat flow was still increasing for Point 11.

5.2.4.1 Discussion

As the pressure during this test was atmospheric, the 2% saturation temperature of CO_2 was lower than during previous tests. The registered heat exchanger temperature never reached the 2% desublimation temperature even though high biogas purity was registered. The incoming refrigerant temperature was however well below this level and this was the reason for the high biogas purity.

48

Compared to Test 2, Test 4 had

- Equal biogas mass flow rate
- Doubled biogas flow velocity
- Halved residence time
- Halved biogas pressure
- Equal HX A temperature

The heat flow in Test 4 was more evenly distributed than in Test 2. This was due to insufficient residence time for the CO_2 to desublimate at the leading edge. The desublimation process therefore occurred further into the heat exchanger, in a more evenly distributed manner. The registered biogas purity during this test was slightly lower, which followed from insufficient biogas residence time. As a matter of fact the desublimation temperature is also lower under a lower pressure, see Figure 8. This contributed to the lower separation efficiency. The decreased pressure also increased the molecular diffusion coefficient as seen in Eq. 16 but the shorter residence time had a larger impact on the separation.

Looking at Test 2 and 4, the amount of CO_2 stored at the lower pressure during Test 4 was about 83% of that in Test 2. This was due to the lower desublimation temperature. The thermal inertia of HX A in this test could be used to desublimate less CO_2 compared to the higher pressure case, since HX A had the same initial temperature.

Compared to Test 3, Test 4 had

- Halved biogas mass flow rate
- Equal biogas flow velocity
- Equal biogas residence time
- Halved biogas pressure
- Equal HX A temperature

The heat flow was similar in Test 4 and Test 3. This means that the biogas flow velocity and residence time were of greater importance for the CO_2 frost distribution than the biogas mass flow rate and pressure. The small increase in heat flow for Point 8 came from the decreased CO_2 desublimation temperature, which postponed the process further towards Point 8, rather than at Point 7.

5.2.5   Test 5

The purpose of Test 5-8 was to determine how the purity of the biogas depends on the heat exchanger temperature. These four tests were started with the same initial settings except for the temperature, but as can be seen from Table 5 the operating conditions changed when the process was started. The initial thermocouple placement from Test 1 was used during this test.

In this test, the average temperature of HX A was -82 °C. The gas composition measurements are shown in Figure 34. Initially there was a peak in the CH_4 concentration but it leveled out rapidly and stabilized at around 80%. As the process continued, the concentration of CH_4 increased steadily. Despite this increase the temperatures in HX A were fairly constant. The process continued until the differential pressure over HX A became too large and the process had to be stopped.
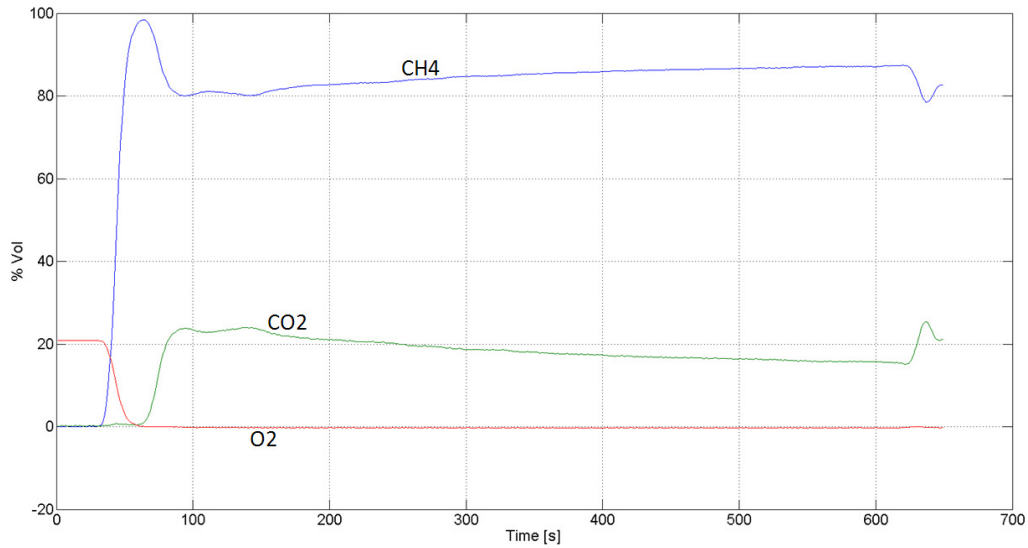
Figure 34 NDIR measurements, Test 5

After about 140 seconds the concentration of CH$_4$ started to increase until it reached 87% and HX A froze up. As can be seen in Figure 35 the incoming temperature of the refrigerant media T4 decreased steadily during the test.
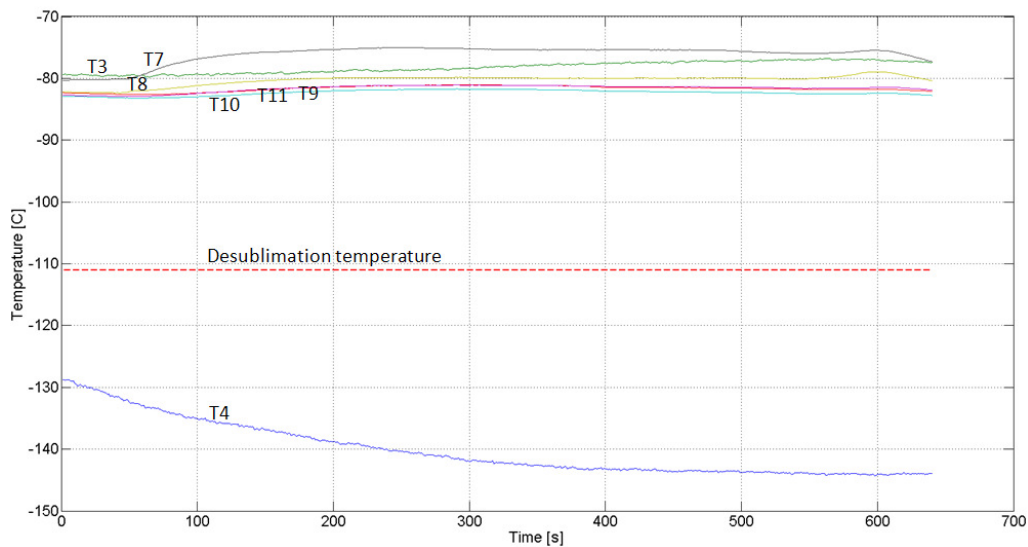
Figure 35 HX A temperature distribution, Test 5

In this test, an even temperature distribution along HX A was achieved. The most significant temperature was at Point 7, 60 seconds after the start of the biogas flow. The total accumulated amount of CO$_2$ in the heat exchanger was found to be 10.1 grams.

5.2.5.1 Discussion

During Test 5 the outlet CH$_4$ concentration increased throughout the run, as shown in Figure 34. This can be compared to the other tests where the concentration instead decreased with time. This was due to the fact that the inlet refrigerant temperature decreased steadily during the test. This resulted in lowered wall temperatures of the

50

plates in HX A. In turn, this led to a decreased temperature of the biogas gas film closest to the wall, resulting in higher separation efficiency.

The initial peak in CH_4 outlet concentration after 60 seconds can be explained by the fact that the initial temperature at Point 7 was sufficiently low to desublimate almost all the incoming CO_2. Figure 35 shows that the temperature at this point rapidly increased once the biogas flow had been started. After a few seconds of operation, the temperature of HX A was not low enough to desublimate all of the incoming CO_2.

5.2.6   Test 6

In this test, the average temperature of HX A was -92 °C. The test was stopped after 560 seconds when the differential pressure over HX A became too large. The gas analyzer measurements are shown in Figure 36 where the biogas purity stayed at a constant level of about 98%. The altered thermocouple placement as used in Test 2 was used during this test.
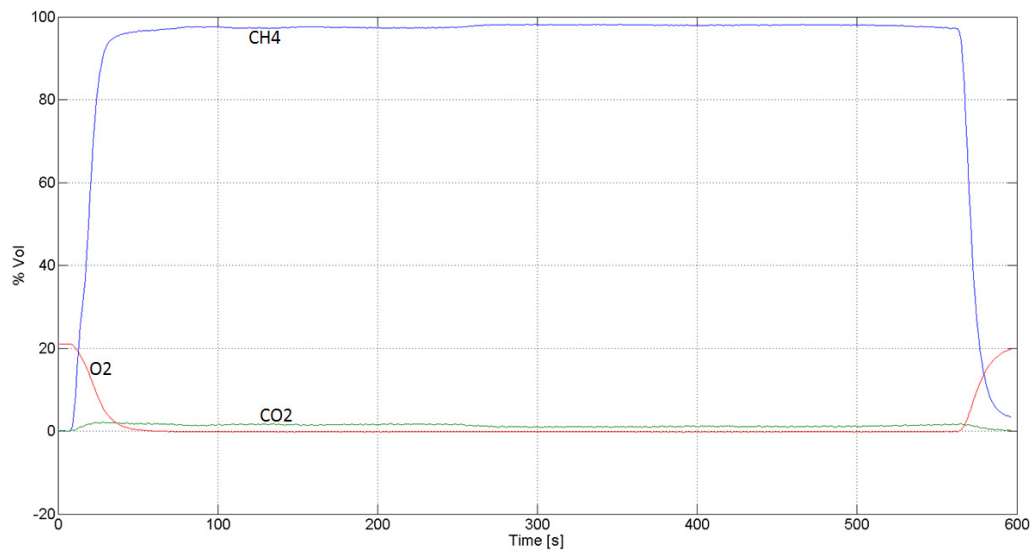
Figure 36 NDIR measurements, Test 6
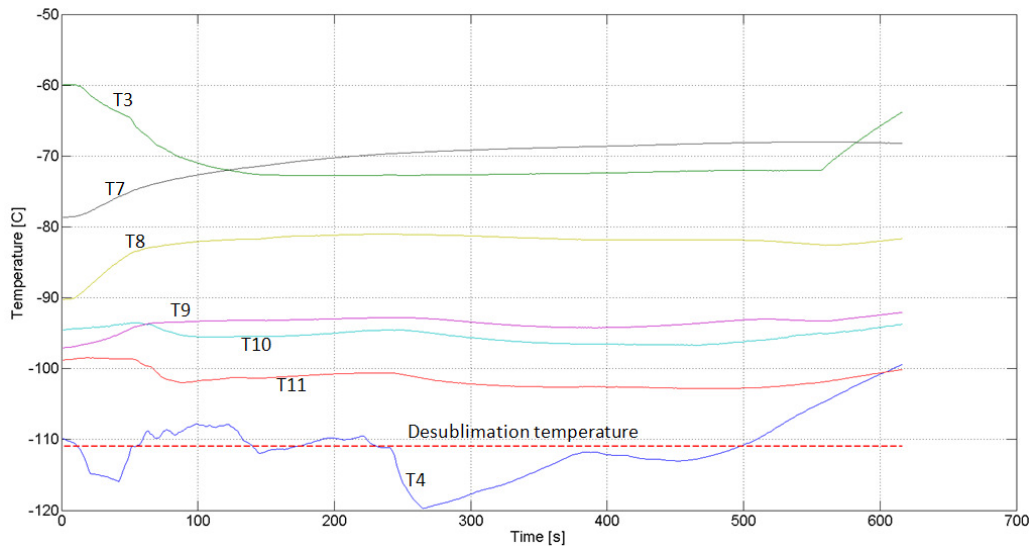
Figure 37 HX A temperature distribution, Test 6

51

As shown in Figure 37, the largest temperature increase after the biogas flow was started can be seen at Point 7 and 8.

A total of 18.2 grams of CO_2 was accumulated during this test.

5.2.6.1 Discussion

The temperature of the five measurement points on the heat exchanger was above the 2% CO_2 desublimation temperature for the entire run. The temperature of the incoming refrigerant was however fluctuating above and below this level. After about 260 seconds the temperature of the incoming refrigerant decreased well below this level. At the same time, the biogas purity increased to a level of around 98%. This means that the last part of the CO_2 was desublimated below Point 11, since T11 was not sufficiently low.

5.2.7 Test 7

In this test, the average temperature of HX A was -102 °C. The purity was found to be high throughout the separation cycle as shown in Figure 38. The decreased purity at approximately t = 120 seconds was caused by an increased temperature of HX A (see lines for T7-T11 in Figure 39). This was momentarily compensated for by an increased refrigerant flow. The initial thermocouple placement from Test 1 was used during this test.
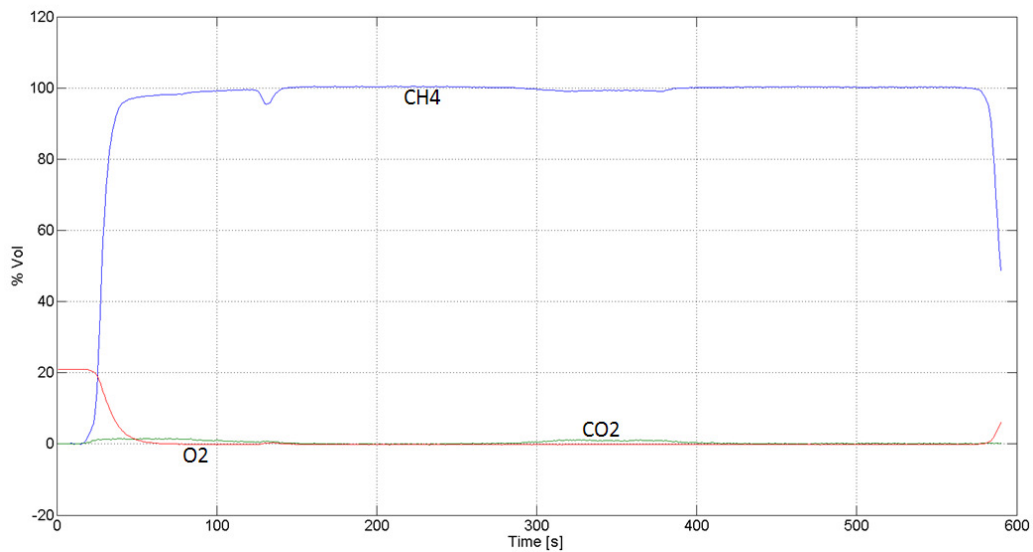
Figure 38 NDIR measurements, Test 7

Between t = 300 and 380 seconds the biogas purity decreased, as shown in Figure 38. This was at the same time as the temperature inside HX A increased, as can be seen in Figure 39. The total accumulated amount of CO_2 in HX A was 15.9 grams.
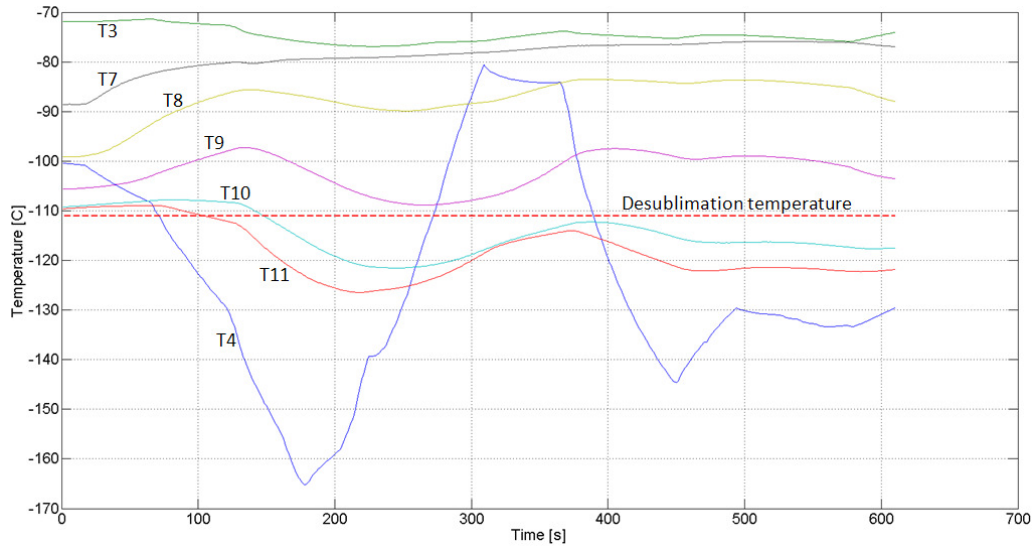
Figure 39 HX A temperature distribution, Test 7

When T4 was above the 2% CO_2 desublimation temperature, the biogas purity decreased somewhat.

5.2.8   Test 8

High biogas purity was achieved using even lower HX A temperature. The initial average temperature of HX A for this test was -110 °C. The test was aborted when HX A froze up by the desublimated CO_2. The initial thermocouple placement from Test 1 was used during this test.

Figure 40 shows the gas composition measurements of the test run. The biogas purity was high, around 100% for the whole run.
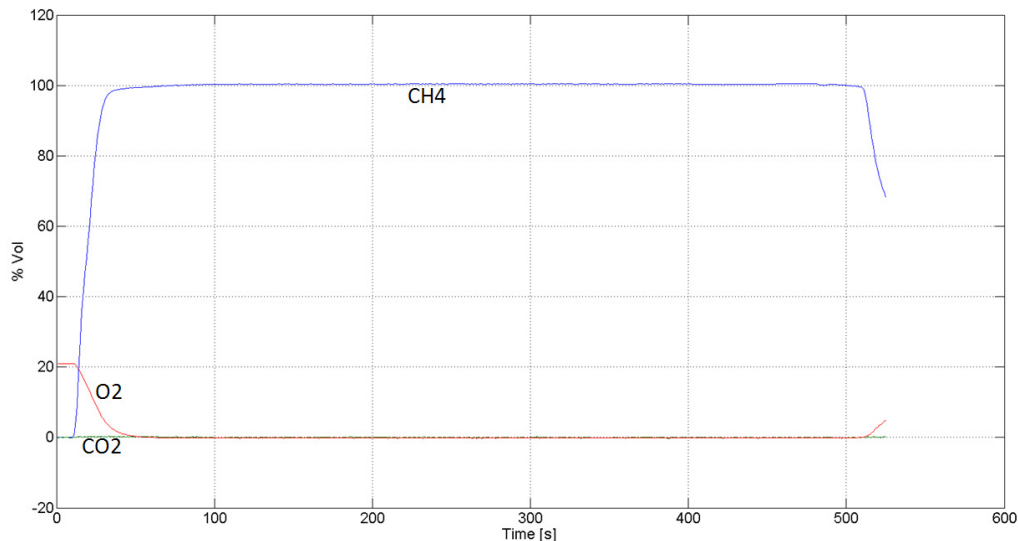
Figure 40 NDIR measurements, Test 8

Figure 41 shows the temperature distribution in HX A during the test run. The total accumulated amount of CO2 in the heat exchanger was 15.7 grams.

53
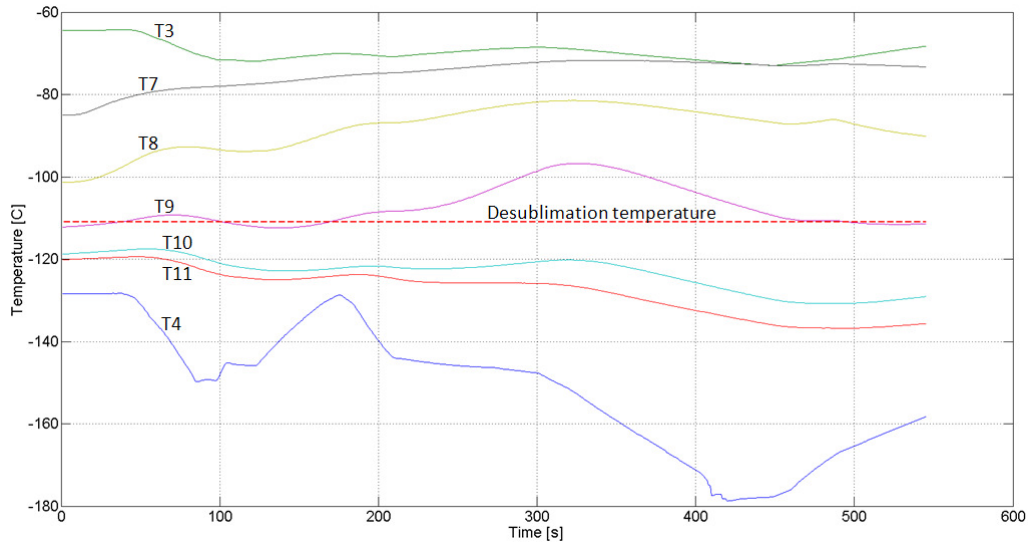
Figure 41 HX A temperature distribution, Test 8

5.2.8.1 Discussion

The results presented for Test 5-8 showed that in order to reach close to 100% biogas purity, a heat exchanger temperature of -102 °C was sufficiently low. The successively decreased temperature resulted in increased CO_2 mass transfer properties. This followed from the lowered saturation concentration as stated in Chapter 3.3. These results apply for the operating conditions used in Test 5-8, with a certain biogas mass flow rate and pressure. The results would however not be the same if the separation process was run under different operating conditions. If the biogas mass flow rate was increased, a lower heat exchanger temperature would be required in order to reach high biogas purity. If the biogas pressure was increased, a higher heat exchanger temperature would be sufficient.

5.3   Process regeneration

The sublimation of CO_2 started when the CO_2 frost layer reached a temperature of around -78 °C, since the regeneration was performed under atmospheric pressure. The mass flow rate of the refrigerant media was kept constant during the regeneration, with a CH_4 flow rate of 16 l_n/min and a N_2 flow rate of 12 l_n/min. During the regeneration, the refrigerant flow was completely bypassed HX B, i.e. the refrigerant was not cooled before entering HX A.

Because of the large thermal inertia of the heat exchanger, some time was needed to heat up HX A to the sublimation temperature of CO_2. As can be seen from Figure 42 the time required from the start of the regenerative cycle until the first amount of CO_2 started to sublimate was around 5 minutes. Since all the regenerative cycles performed were very similar in time as well as temperature distribution, only one is presented here. A typical regeneration cycle needed around 30 minutes to finish, i.e. to sublimate all the accumulated CO_2 frost. Initially there was also a small amount of trapped CH_4 leaving the system.

54
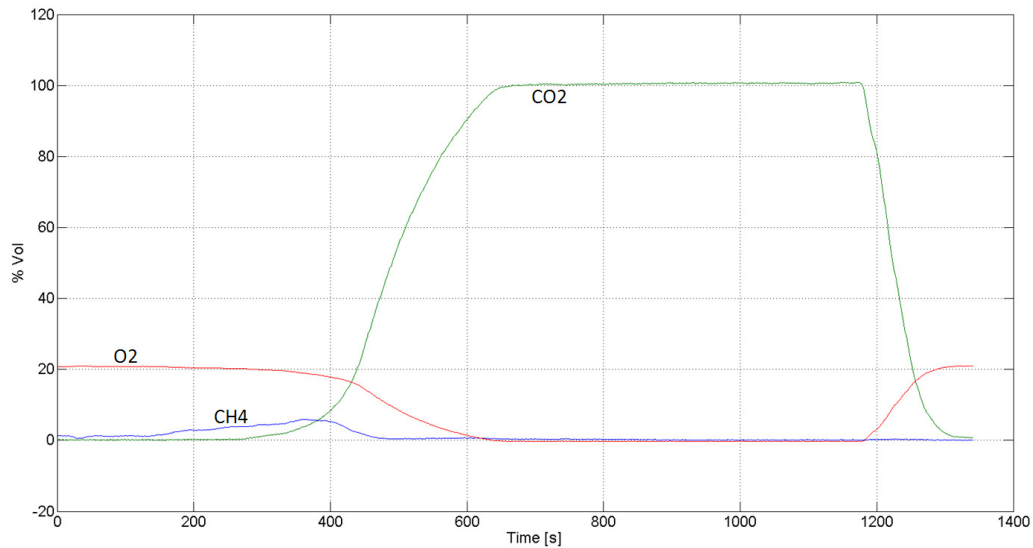
Figure 42 Regenerative cycle, NDIR measurements

Figure 43 shows the temperature distribution in HX A. The temperatures that increased first were T11 and T10, which are located furthest down HX A. These were later followed by the temperatures T9, T8 and finally T7. This was to be expected, mainly due to the fact that the refrigerant media entered HX A counter-currently and heated up the lower parts first.
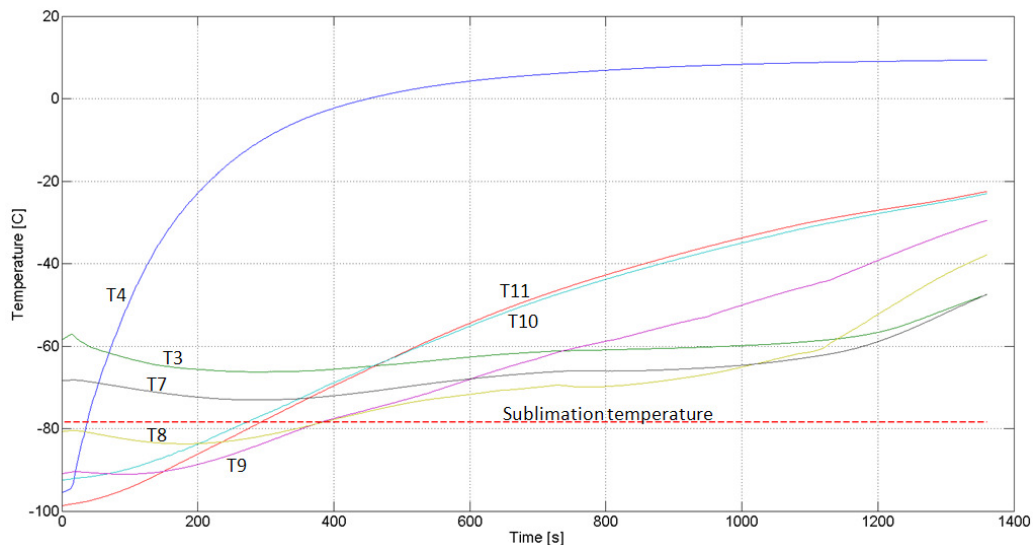
Figure 43 Temperature in HX A during regeneration

During the first 200 seconds the temperatures at the top of HX A, primarily T7 and T8, decreased. This was due to that the temperature of the incoming refrigerant media was cooled below the temperature of T7 and T8 by the lower parts of HX A before reaching the upper parts of the exchanger.

5.3.1.1 Discussion

During the first period in Figure 42, HX A was still colder than the sublimation temperature of CO_2. After about 180 seconds a small stream of methane started to pass through the analyzer. When HX A froze up and the biogas flow was stopped,

there was CH_4 trapped inside the system. As the temperature of the heat exchanger increased during the regenerative process, the density of the gas decreased and the CH_4 was therefore pushed out.

After about 300 seconds the heat exchanger reached high enough temperature to initialize the sublimation of the frozen CO_2. After this point the flow of sublimated CO_2 increased rapidly until the concentration reached 100%. After 1300 seconds of regeneration all the CO_2 had been sublimated, and the test rig was ready for the next cool-down cycle to begin.

The slopes of the curves in Figure 43 can be used as an indication to where the CO_2 was accumulated. A steeper slope indicates that the refrigerant media was able to heat up HX A quicker and that there was less CO_2 at that position using heat for sublimation. The temperature at Point 10 and 11 increased at an almost constant pace throughout the entire regeneration process. This was due to that a relatively small amount of CO_2 frost was accumulated here. Otherwise it would have shown up as a change in the slope when no CO_2 was remaining to absorb the heat. The temperature increase at Point 9 was almost constant until after about 950 seconds, and later at 1125 seconds, where it started to increase faster. After 1125 seconds there was therefore no more CO_2 frost at that position. The same is valid for Point 8 which also had a temperature increase at 1125 seconds. The last point to have a sudden increase in temperature was Point 7, which would suggest that the main part of the remaining CO_2 was located there. This CO_2 distribution profile is also supported by experiments performed by other researchers, as shown in Chapter 3.3.

Running the separation process with lower HX A temperature means that the temperature needs to be increased more in order to regenerate it, resulting in a longer regeneration time. The sublimation temperature of CO_2 increases with increasing pressure. For pure CO_2 under atmospheric pressure the sublimation temperature is -78.5 °C while at 3 bar it is -64 °C. When using higher biogas pressure during separation a higher heat exchanger temperature is sufficient to still achieve high CO_2 desublimation efficiencies. It follows that when the regenerative process is started and the pressure is decreased to atmospheric level, a smaller temperature increase is required in order to start sublimation. This results in a shorter regeneration time. If the pressure during regeneration instead is higher than atmospheric level, the regeneration time will be longer.

By using a large pressure difference between separation and regeneration, the pressure swing principle can be used, i.e. when the change in pressure is used for the purpose of altering the CO_2 sublimation temperature. If the pressure swing is large enough, the temperature of the heat exchanger does not have to be increased in order to start CO_2 sublimation. This decreases the time required to complete the regeneration cycle. For instance, a vacuum pump can be used to decrease the pressure and enhance the sublimation process. This would although result in increased investment costs and further complexity of the upgrading rig.

56

6   Discussion

Test rig equipment

There were two additional thermocouples not mentioned within the results chapter, namely the ones placed on the incoming and outgoing biogas stream (T1 and T2). Since the separation process was only run for a relatively short period of time, the thermal inertia of the copper tubing dominated during the process. Therefore the temperatures at those points never had time to stabilize.

The thermocouples T7 to T11 were placed both on the back and on the side of the heat exchanger. Both configurations were tested. When the thermocouples were placed on the back they measured the temperature of the refrigerant media more directly, since the refrigerant was on the other side of the back plate. The refrigerant flow was mixed well enough by the corrugations inside HX A to give a quick response to the temperature changes caused by the biogas flow. Thanks to this, the temperature profiles presented for Test 1, 5, 7 and 8 gave a clear indication about what happened to the temperature at the next plate where the refrigerant met the gas flow.

The thermocouples were about one centimeter long and when placed on the side of HX A they extended to measure over several plates. The thermocouples therefore measured an average value over these plates and also over both the biogas stream and the refrigerant stream. No difference in temperature profiles could be seen between the two different thermocouple setups.

Test experiences

The highest biogas pressure the rig was tested for was 2 bar absolute pressure. When using higher pressure, the fluctuations in the flow of biogas were too large to achieve stable operation.

At some points in the heat exchanger the temperature was lower than the average temperature, and in other parts higher. The CO_2 that was not successfully captured upstream where the heat exchanger temperature was higher than the desublimation temperature was instead captured downstream where the temperature was lower than the desublimation temperature. Near the biogas inlet the temperature of the plates was above the average HX A temperature during the performed tests. Having isothermal plates in HX A would result in more accumulation closer to the leading edge.

The heat losses to the test rig from the surroundings before the start of the biogas flow was measured to around 11 W. This was a significant amount since the heat demand from the separation process during the performed tests was about 23 W. These large heat losses followed from the fact that most tubing was not insulated and a lot of humidity from the air condensed and froze onto the tubes.

Test rig improvements

Larger upgrading capacity requires more heat transfer surface and therefore larger heat exchangers. By increasing the number of plates in HX A the biogas flow is divided into a larger number of streams. This increases the heat exchanger area but decreases the flow velocity. In order to ensure even CO_2 accumulation across the heat exchanger plates, the biogas flow velocity needs to be increased. This is done by increasing the biogas mass flow rate.

By increasing the heat exchanger plate length and also increasing the biogas flow velocity, the CO_2 becomes evenly distributed while still maintaining high separation efficiency due to the longer residence time.

It is possible to liquefy the CO_2 while still extracting CH_4 in gaseous phase. A continuous drain of liquefied CO_2 eliminates the problem with the heat exchanger freezing up. Liquefying CO_2 requires process pressures of at least 10 bar. Thus in order to make liquefaction possible, high pressure equipment is needed.

Cycle running time

Heating up HX A to sublimation temperature makes up a major part of the time required for the regeneration cycle. The upgrading process can be made more time efficient by running the separation cycle for as long as possible. By doing this, the regeneration cycle takes a smaller proportion of the total time.

A larger pressure "swing" can be used to reduce the time needed to increase the temperature of HX A to sublimation temperature. A larger part of the regeneration time will thus be used for the actual sublimation of CO_2.

By using two or more heat exchangers in parallel operation, one heat exchanger can desublimate CO_2 and freeze up, while the other one is being regenerated. In this way, the process does not need to be stopped because of heat exchanger freeze up.

The separation cycle time is limited by the time until heat exchanger freeze up. A high frost layer density is desirable in order to prolong the time until the frost layer grows thick enough to hinder the biogas flow. As shown in Chapter 3.3, the density of the frost layer depends on several factors. The factors resulting in increased CO_2 frost layer density are; a low plate temperature, a high flow velocity and a high pressure. By performing the separation under these conditions the cycle running time can be increased.

Biogas temperature and CO$_2$ frost distribution

The desublimation temperature of CO$_2$ decreases with decreasing partial pressure, as mentioned in Chapter 3.3. This means that when the biogas enters the heat exchanger with a composition of 40% CO$_2$ and 60% CH$_4$, a temperature of -80 °C is required to desublimate the first amount of CO$_2$.

In order to freeze out CO$_2$ evenly across the heat exchanger surface, the biogas should be successively cooled. By cooling the biogas along the CO$_2$ saturation curve with a constant decrease in concentration, from 40% down to 1%, an even CO$_2$ frost layer will be formed. At 2 bar absolute biogas pressure this means that the CO$_2$ partial pressure should decrease from 0.8 bar to 0.02 bar. The corresponding temperature curve is shown in Figure 44.
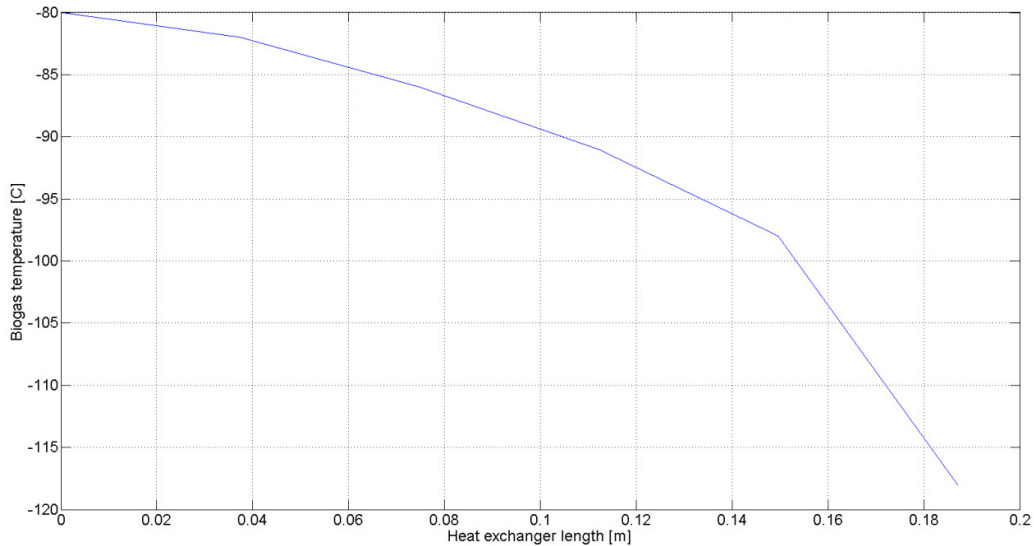
Figure 44 Biogas cooling curve for an even CO$_2$ distribution

The temperature is plotted for a heat exchanger length of 187 mm since that was the length of HX A. The temperature profile shows what temperature the biogas should have at each point in the heat exchanger, however the temperature of the heat exchanger has to be below this level.

The biogas enters the heat exchanger at around 20 °C and in order for it to reach -81 °C at the beginning of the plate, the heat exchanger temperature at the upper part has to be significantly lower than this. Another option is to pre-cool the biogas to a temperature of around -70 °C before it enters the separation heat exchanger. This would make the required heat exchanger temperature distribution more similar to that in Figure 44. The temperature of the heat exchanger would although have to be lower in order to have sufficient thermal driving force.

7   Conclusions

Separation

Biogas purity exceeding 99% was measured and proven to be achievable during continuous operation for a time period of around 9 minutes.

The upgraded biogas purity is highly dependent on the temperature of the heat exchanger. In order to reach 99% biogas purity, the lowest temperature in the heat exchanger has to be below -118 °C.

Higher biogas flow velocity results in a more evenly distributed CO_2 frost layer. Reduced biogas residence time results in lower separation efficiency.

The biogas purity is higher when running the separation process with higher biogas pressure, compared to using lower pressure. An increased biogas pressure reduces the need for a low heat exchanger temperature. A high biogas pressure during separation also enables the pressure swing principle to be used for regeneration, reducing the need for unnecessary heating of HX A.

Heat exchanger regeneration

The time required for one regeneration cycle is large compared to the time for one separation cycle.

The regeneration time is reduced by

- A small temperature difference between the temperature of the heat exchanger during the previous separation cycle and the sublimation temperature during the regeneration cycle
- A high temperature and flow rate of the regenerative refrigerant
- A low pressure inside HX A

If the pressure swing principle is not used, having a heat exchanger with small heat capacity also reduces the regeneration time.

8 References

1. **M. Valleskog, Å. Marbe, L. Colmsjö.** *System- och marknadsstudie för biometan (SNG) från biobränslen.* Sweden : Svenskt Gastekniskt Center AB, SGC185, March 2008, Malmö, 2008.

2. **K. Christensson, L. Björnsson, S. Dahlgren et.al.** *Gårdsbiogashandbok.* Sweden : Svenskt Gastekniskt Center, SGC Report No. 206, 2009.

3. **M. Persson.** *Utvärdering av uppgraderingstekniker för biogas.* Sweden : Svenskt Gastekniskt Center, SGC Report No 142, Malmö, 2003.

4. **J. T. Yeh, H. W. Pennline.** *Study of CO2 Absorption and Desorption in a Packed column.* USA : National Energy Technology Laboratory, U.S. Department of Energy, 2001.

5. **J. Benjaminsson, N. Johansson, J. Karlsvärd.** *Deponigas som fordonsbränsle.* Sweden : Svenskt Gastekniskt Center, SGC Report 214, 2010.

6. **N. Tippayawong, P. Thanompongchart.** *Biogas quality upgrade by simultaneous removal of CO2 and H2S in a packed column reactor.* Department of mechanical Engineering, Chiang Mai University, Thailand : s.n., 2010.

7. **Eindhoven, J de Hullu, J.I.W. Maaseen, P.A van der Meel, S. Shazad, J.M.P. Vaessen.** *Comparing different upgrade techniques.* Holland : Interim report, DMT, Technische Universiteit, 2008.

8. **C. A. Grande, A. E. Rodrigues.** *Electric Swing Adsorption for CO2 removal from flue gases.* Portugal : Department of Chemical Engineering, University of Porto, 2007.

9. **M. Harasimowicz, P. Orluk, G. Zakrzewska-Trznadel, A.G. Chmielewski.** *Application of polyimide membranes for biogas purification and enrichment.* s.l. : Journal of Hazardous materials, nr. 144, p. 698-702., 2007.

10. **S. Atchariyawut, R. Jiratananon, R. Wang.** *Separation of CO2 from CH4 by using gas-liquid membrane contacting process.* Thailand : Department of Chemical Engineering, King Mongkut's University of Technology, Bangkok, 2007.

11. **R. Xing, W.S. Winston Ho.** *Synthesis and characterization of crosslinked polyvinylalcohol/polyethyleneglycol blend membranes for CO2/CH4 separation.* s.l. : Journal of the Taiwan Institute of Chemical Engineers, nr. 40, p.654–662, 2009.

12. **M. Hagen, E. Polman, J. K. Jensen, A. Myken, O. Jönsson, A. Dahl.** *Adding gas from biomass to the gas grid.* s.l. : Swedish Gas Center, SGC Report No. 118, 2001.

13. **A. Hart, N. Gnanendran.** *Cryogenic CO2 Capture in Natural Gas.* s.l. : Energy Procedia 1, pp. 697-706, 2009.

14. **L. Deng, M. Hägg.** *Techno-economic evaluation of biogas upgrading process using CO2 facilitated transport membrane.* s.l. : International Journal of Greenhouse Gas Control 4 pp. 638–646, 2010.

15. **N. Johansson.** *Production of liquid biogas, LBG, with cryogenic and conventional upgrading technology.* Lund, Sweden : Lund University, 2008.

16. **Benjaminsson, J.** *Nya renings- och uppgraderingstekniker för biogas.* Malmö, Sweden : Swedish Gas Center, SGC Report No. 163, 2006.

17. **http://www.todaystrucking.com/news.cfm?intDocID=23071.** *Volvo first to market with methane-diesel engines.* s.l. : Today's Trucking, 2010.

18. **A. Pettersson, M. Losciale, S. Liljemark.** *Möjligheter med LNG i fordonsgasförsörjningen i Sverige.* Sweden : Svenskt Gastekniskt Center AB, SGC167, September 2006, Malmö, 2006.

19. **M. Marsh.** *A Sourcebook for the Production and Use of Renewable Natural Gas in California.* USA : Report for Western United Dairymen, 2005.

20. **K. Loubar, C. Rahmouni, O. Le Corre, M. Tazerout.** *A combustionless determination method for combustion properties of natural gases.* s.l. : Fuel, nr. 86, p. 2535 – 2544, 2007.

21. **H. Thunman.** *Combustion Engineering.* Sweden : Chalmers University of Technology, 2010, Göteborg, 2010.

22. **J. Card, L. Hoseong.** *Leading technology for next generation LNG carriers.* Korea : From proceedings of the fifteenth international offshore and polar engineering conference, June 19-24, 2005, Seoul, 2005.

23. **A. Pettersson, M. Losciale, S. Liljemark.** *LCMG – Pilotprojekt för LMG som fordonsbränsle i Sverige.* Sweden : Svenskt Gastekniskt Center, SGC Report No. 177, 2007.

24. http://www.chemicalogic.com/download/co2_phase_diagram.pdf. [Online] [Cited: 03 22, 2011.] ChemicaLogic Corporation.

25. http://encyclopedia.airliquide.com/images_encyclopedie/VaporPressureGraph/ Carbon_dioxide_Vapor_Pressure.GIF. [Online] [Cited: 05 30, 2011.] Air Liquide Gas Encyclopedia.

26. **V. N. Schelkunov, N. Z. Rudenko, Yu. V. Shostak, V. I. Dolganin.** *Surface desublimation of carbon dioxide from binary gas mixtures.* Ukrain : Academy of Sciences of the Ukrainian SSR, 1987.

27. **H. Chang, M. J. Chung, S. B. Park.** *Cryogenic Heat-Exchanger Design for Freeze-out Removal of Carbon Dioxide from Landfill Gas.* s.l. : Journal of Thermal Science and Technology, Vol 4, No. 3, 2009, 2009.

28. **F. Incropera, D. Dewitt, T. Bergman, A. Lavine.** *Fundamentals of Heat and Mass Transfer, 6th edition.* USA : Hoboken, NJ, John Wiley & Sons Inc., 2007.

29. **A. Cooper, J.D. Usher.** *Plate heat exchangers, Heat Exchanger-Design Handbook.* USA : Hemisphere publishing, Chap 3.7, New York, 1983.

30. http://www.technoserviceco.com/contain/gasketfig1.gif. [Online] [Cited: 02 02, 2011.] Techno Service Co.

31. **S.W. Churchill, H. H. S. Chu.** s.l. : International Journal of Heat and Mass Transfer 18, p. 1323, 1975.